Composite Structures 327 (2024) 117645

Contents lists available at ScienceDirect

Composite Structures

journal homepage: www.elsevier.com/locate/compstruct

Additive manufacturing error quantification on stability of composite sandwich plates with lattice-cores through machine learning technique

Weizhe Tian, Qingya Li, Qihan Wang *, Da Chen, Wei Gao *

Centre for Infrastructure Engineering and Safety (CIES), School of Civil and Environmental Engineering, The University of New South Wales, Sydney, NSW 2052, Australia

ARTICLE INFO

Keywords:
Additive manufacturing
Virtual modelling technique
Lattice-core composite sandwich plate
Stability analysis
Multiscale analysis

ABSTRACT

Architected lattice structures are designed to achieve specific mechanical properties while maintaining relative lightweight. Additive Manufacturing (AM) facilitates the fabrication of lattice structures with complex geometries. However, manufacturing imperfections, e.g., node dislocation, radius variation, and waviness, inevitably affect the performance of composite structures, of which the impact is significant yet difficult to quantify. Herein, a virtual model-assisted AM error quantification scheme is proposed to alleviate this challenge. The influence of geometric imperfections on the static buckling behaviour for sandwich lattice-core panels is investigated. A recently developed Extended Support Vector Regression (X-SVR) is utilized to alternatively bridge multiscale analyses. By integrating the sampling and virtual modelling methods, the effect of AM errors can be comprehensively quantified with statistical moments, probability density function (PDF), cumulative distribution function (CDF), etc. Furthermore, high computational efficiency, robustness, and other inherent features highlight the applicability of the proposed AM error quantification scheme in engineering.

1. Introduction

Artificial architected lattice materials are a type of cellular structure that mimic the natural design of human bones, plant stems, wood, cork, and other biological materials [1–4]. These materials exhibit remarkable mechanical properties such as a high stiffness-to-weight ratio, excellent energy absorption, and low thermal conductivity [5–9], which make them suitable for various engineering applications in the automotive, aerospace, biomedical, and construction sectors [10–13]. As an emerging technique, Additive Manufacturing (AM) refers to a fabrication process by adding material in a successive manner [14,15], which promotes the development of material science and is used to build cellular structures with geometric complexities [16–20]. Particularly, Selective Laser Melting (SLM) is one of the commonly used techniques in Metal Additive Manufacturing (MAM) [21] to provide engineers with economical and effective access to the fabrication of metallic lattice materials [22–24]. Therefore, AM techniques have achieved widespread applications and possess great potential in multiple disciplines including biomedical, aerospace, mechanical engineering, etc. [25–28].

However, the lattice structures fabricated by AM techniques inevitably introduce geometric imperfections, which are termed as the offset of junction center position (strut node dislocation), the variation of strut cross-section radius (radius variation), and the offset of cross-section center positions (waviness) [23,29,30]. A number of studies have been conducted to explore the influence of imperfections on additively manufactured lattice structures. Lozanovski et al. [21] utilized the finite element method (FEM) and proposed a computer-aided design (CAD) model involving the strut defects to explore the mechanical response of lattice structures. Lei et al. [31] and Cao et al. [32] conducted compressive experiments and evaluated the influence of SLM-induced imperfections on the compressive performance, energy absorption capability, mechanical properties, and deformation mechanisms of lattice structures. Dallago et al. [29] combined X-ray computed tomography with the FEM to investigate the fatigue strength and elastic modulus of SLM lattice structures. Liu et al. [30] utilized CT tomography to develop numerical models and studied the role of SLM-induced imperfections on the elastic response and failure mechanism of the octet and rhombicuboctahedron lattice structures. Cumulative research has continuously revealed that the aforementioned AM errors could have significant impacts: without appropriate consideration of these errors, the mechanical properties of products may vary dramatically, leading to possible structural failures. Thus, to provide a feasible approach to

* Corresponding authors.
E-mail addresses: qihan.wang@unsw.edu.au (Q. Wang), w.gao@unsw.edu.au (W. Gao).

https://doi.org/10.1016/j.compstruct.2023.117645
Received 9 June 2023; Received in revised form 21 September 2023; Accepted 21 October 2023
Available online 31 October 2023

quantify the effects of AM errors on composite lattices for real-world adoptions, an advanced and systematic framework is expected to be developed.

The buckling behaviour [33], as a fundamental mechanical performance, is investigated through the numerical homogenization method [34,35] and the first-order shear deformation theory (FSDT) [6,36]. A probabilistic statistical model used to model structural imperfections [30] is adopted herein to evaluate the concerned AM errors. By considering these errors as independent probabilistic statistical variables, the homogenized mechanical properties in mesoscale lattice components, e.g., Young's modulus, Poisson's ratio, etc., possess the characteristics of randomness that may be reflected in the structural behaviours, such as the critical buckling load. Although sufficient statistical information on the concerned structural response can be obtained through the brute Monte Carlo Simulation (MCS) method, the expensive computational costs are still a great concern in real-world engineering problems. Thus, to facilitate the quantification of the effects of AM errors in a computationally effective and efficient manner, an advanced analysis method is proposed by integrating the sampling method with machine learning and data processing techniques. Inspired by several successes achieved in uncertainty quantification and reliability analysis for various types of engineering structures [37–40], a recently developed supervised machine learning technique, namely, Extended Support Vector Regression (X-SVR), is adopted to alternatively express the originally underpinned and sophisticated relationship between AM errors and the concerned structural performance, i.e., bulking load. Due to the inherent features of convex optimization programming, the embedded X-SVR technique can theoretically achieve a good performance in regression. Based on the established X-SVR model, the sampling method can be implemented with greatly reduced computational costs. A sufficient amount of statistical information on the quantity of interest can be obtained, including not only the statistical moments (means, standard deviations, etc.), but also the probability density function (PDF), and cumulative distribution function (CDF). Generally, the advantages of the proposed advanced AM error quantification framework through machine learning techniques can be summarized as follows:

(1) Wide applicability: The proposed AM error quantification framework supports the consideration of various types of lattice-core composite structures, e.g., cubic center, octet, vintiles, etc. Moreover, diverse critical AM errors, such as strut node dislocation, radius variation, waviness, etc., are included.

(2) Unrestricted selection of quantities of inputs and outputs: There is no obvious restricted selection of quantities of both inputs and outputs within the system. Moreover, according to the statistical information from reality, AM errors can be described as statistical models, and characterized by appropriate statistical moments and distribution types within the proposed quantification framework.

(3) High compatibility: Data processing techniques, e.g., clustering strategy, normalization, feature selection, etc., as well as other machine learning techniques, can be easily integrated within the proposed quantification framework.

(4) Computational efficiency: By implementing the sampling-based method on the established virtual model that can be expressed as an explicit formulation, the computational costs and resources can be remarkedly reduced.

(5) Adequate statistical information: Based on the sampling-based method, a sufficient amount of statistical information of any concerned structural response can be effectively obtained, including the statistical moments, PDF, and CDF.

In addition to these merits, information update, hypothesis analysis, and sensitivity analysis can be effectively and efficiently implemented on the established virtual models. Generally, the proposed AM error quantification strategy can be employed to investigate the sophisticated mechanisms between these imperfections induced by the manufacturing, processing, assembling, etc., in micro or mesoscale to overall structural performance, and convincingly, it possesses great potential for the wide adoption in advanced manufacturing and composites engineering.

The remainder of this paper is organized as follows: Section 2 presents the preliminaries, including the static buckling analysis for lattice-core composite plates with either 'error-free' geometries or AM errors. In Section 3, the proposed machine learning-assisted AM error quantification strategy is thoroughly presented. Numerical investigations for lattice-core composite plates under the three types of AM errors are subsequently implemented in Section 4 to demonstrate the applicability and computational efficiency of the proposed strategy. Finally, conclusions are drawn in Section 5.

2. Preliminaries

This paper aims to quantify the influence induced by AM errors on the static buckling behaviour of additively manufactured architected lattice-core composite sandwich plates under simply supported and clamped boundary conditions. Three commonly encountered imperfections, especially raised by the SLM technique, including the strut node dislocation, radius variation, and waviness, are considered. The stability of composite sandwich plates, which consist of a Ti-6Al-4V architected lattice-core layer bounded by top and bottom aluminium isotropic face layers, are investigated under uniaxial loading conditions. This section elaborates on this problem by detailing the static buckling analysis for lattice-core composite sandwich plates with 'error-free' geometry, as well as that involving AM errors.

2.1. Static buckling analysis for lattice-core composite sandwich plates with 'error-free' geometry

Herein, three types of lattice materials (i.e., the octet, cubic center, and vintiles), commonly applied to compose the core layer of composite sandwich plates in engineering industries [6], are selected in this static buckling analysis. Their detailed topologies are depicted in Fig. 1.

Fig. 2 presents the modelling of the lattice-core composite sandwich plate and gives the corresponding topology and dimensional information. The plate length and width are denoted by L_a and L_b, respectively. The thicknesses of the face layer, the core layer, and the composite sandwich plate are represented as h_f, h_c and h, respectively. Two well-known methodologies, numerical homogenization and FSDT, are adopted and used to calculate the homogenized material properties and to generate the governing equation for solving the static buckling load of the composite sandwich plate. The following part will briefly introduce these two methodologies, as well as the governing equations. More detailed derivations can be found in [6] and [34].

In terms of the homogenization method for periodic composite materials, the homogenized elasticity tensor E^H_{ijkl} can be computed as:

$$E^H_{ijkl} = \frac{1}{|Y|}\int_Y E_{pqrs}\left(\varepsilon^{0(ij)}_{pq} - \varepsilon^{(ij)}_{pq}\right)\left(\varepsilon^{0(kl)}_{rs} - \varepsilon^{(kl)}_{rs}\right)dY \tag{1}$$

where E_{pqrs} is defined as the locally varying elasticity tensor, $|Y|$ indicates the unit cell volume. $\varepsilon^{0(ij)}_{pq}$ and $\varepsilon^{0(kl)}_{rs}$ are prescribed strain fields. $\varepsilon^{(ij)}_{pq}$ and $\varepsilon^{(kl)}_{rs}$ are locally varying strain fields.

The homogenization equation should be discretised and solved by FEM, which is often called numerical homogenization. Grounded on the FEM, the strain ε and the element stiffness matrix K_e can be expressed as:

$$\varepsilon^{(ij)} = BU^{(ij)}, K_e = \int_{V_e} BEB^T dV_e \tag{2}$$

where B represents the strain–displacement matrix, which is defined as the derivative of element shape function.

The material design domain is assumed to be discretised by N finite elements, where the type of each finite element is hexahedron with the

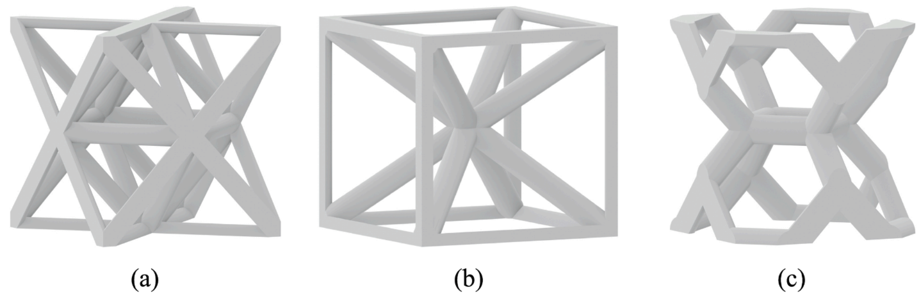

Fig. 1. Lattice materials (a) octet; (b) cubic center; (c) vintiles.

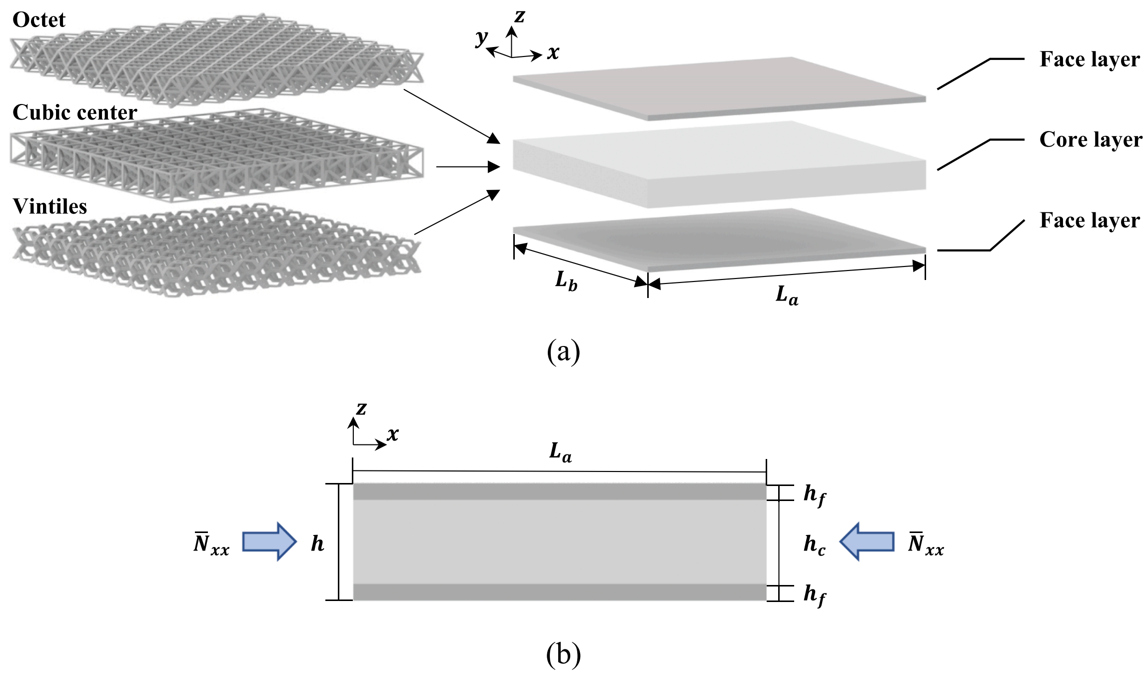

Fig. 2. The schematic diagram of the lattice-core composite sandwich plate subjected to uniaxial loading (a) 3D model (b) 2D model.

volume of V_e. By substituting Eq. (2) into Eq. (1), the original governing equation in homogenization method can now be expressed in the form of numerical homogenization, which can be expressed in Eq. (3) for calculating the homogenized material properties.

$$C^H_{ijkl} = \frac{1}{|Y|}\sum_{e=1}^{N}\int_{V_e}\left(U^{0(ij)}_{(e)} - U^{(ij)}_{(e)}\right)^T K_e\left(U^{0(kl)}_{(e)} - U^{(kl)}_{(e)}\right)dV_e \tag{3}$$

where C^H_{ijkl}, $U^0_{(e)}$, $U_{(e)}$ and K_e are defined as the homogenized constitutive matrix, the prescribed displacement field, the locally varying displacement field, and the element stiffness matrix, respectively. Then, based on the generalized Hook's law, the homogenized material properties (namely, Young's modulus (E), Shear modulus (G), and Poisson's ratio (v)) can be calculated by the homogenized compliance matrix, which can be obtained by inversing the homogenized constitutive matrix.

Based on FSDT, the stress resultants $\mathbf{N} = [N_{xx}\ N_{yy}\ N_{xy}]^T$, $\mathbf{M} = [M_{xx}\ M_{yy}\ M_{xy}]^T$, and the transverse force resultants $\mathbf{Q} = [Q_x\ Q_y]^T$ can be written as the constitutive relations, and the shear correction factor K_s takes the value of 5/6.

$$\begin{Bmatrix}\mathbf{N}\\ \mathbf{M}\end{Bmatrix} = \begin{bmatrix}\mathbf{A} & \mathbf{B}\\ \mathbf{B} & \mathbf{D}\end{bmatrix}\begin{Bmatrix}\boldsymbol{\varepsilon}_0\\ \boldsymbol{\varepsilon}_1\end{Bmatrix},\ \mathbf{Q} = K_s\mathbf{A}_s\boldsymbol{\gamma} \tag{4}$$

$$\begin{aligned}\left(\mathbf{A},\mathbf{B},\mathbf{D}\right) &= \sum_{k=1}^{3}\int_{z_k}^{z_{k+1}}\mathbf{L}^{(k)}\left(1, z, z^2\right)dz,\\ \mathbf{A}_s &= \sum_{k=1}^{3}\int_{z_k}^{z_{k+1}}\mathbf{L}_s^{(k)}dz\end{aligned} \tag{5}$$

$$\mathbf{L} = \begin{bmatrix}Q_{11} & Q_{12} & 0\\ Q_{12} & Q_{22} & 0\\ 0 & 0 & Q_{66}\end{bmatrix}, \mathbf{L}_s = \begin{bmatrix}Q_{55} & 0\\ 0 & Q_{44}\end{bmatrix} \tag{6}$$

where the elastic constants for the k^{th} layer can be written as:

$$\begin{aligned}Q^k_{11} &= Q^k_{22} = \frac{E_k}{1 - v_k^2},\\ Q^k_{12} &= \frac{v_k E_k}{1 - v_k^2},\\ Q^k_{44} &= Q^k_{55} = Q^k_{66} = \frac{E_k}{2(1 + v_k)}\end{aligned} \tag{7}$$

in which the E_k and v_k represent Young's modulus and Poisson's ratio for the k^{th} layer of the composite sandwich plate.

For the solution of the critical buckling load, assuming the uniaxial in-plane force $\bar{N}_{xx}$ applied along the plate length, the governing equation is consequently obtained:

$$(\boldsymbol{\Gamma}+\boldsymbol{\Lambda})\boldsymbol{\Delta}=\mathbf{0} \tag{8}$$

where:

$$\boldsymbol{\Gamma}=\begin{bmatrix}\Gamma_{11} & \Gamma_{12} & \Gamma_{13}\\ \Gamma_{21} & \Gamma_{22} & \Gamma_{23}\\ \Gamma_{31} & \Gamma_{32} & \Gamma_{33}\end{bmatrix},\ \boldsymbol{\Delta}=\begin{Bmatrix}W_{mn}\\ \Theta^{x}_{mn}\\ \Theta^{y}_{mn}\end{Bmatrix},\quad \boldsymbol{\Lambda}=\begin{bmatrix}\overline{N}_{xx}\Gamma_{N11} & 0 & 0\\ 0 & 0 & 0\\ 0 & 0 & 0\end{bmatrix},\ \mathbf{0}=\begin{Bmatrix}0\\0\\0\end{Bmatrix} \tag{9}$$

W_{mn}, Θ^{x}_{mn}, Θ^{y}_{mn} are the arbitrary parameters. Γ_{N11} should be determined by the admissible functions $X_m(x)$ and $Y_n(y)$. The formulations of $X_m(x)$ and $Y_n(y)$ under simply supported (SSSS) and clamped (CCCC) boundary conditions are provided in Eqs. (A1) and (A2) in Appendix A, respectively. Then, the formulation for calculating Γ_{N11} based on $X_m(x)$ and $Y_n(y)$ are given in Eq.(A3). For the coefficients in the matrix $\boldsymbol{\Gamma}$, they should be calculated based on the above-mentioned admissible functions and the coefficients in matrices $\mathbf{A},\mathbf{B},\mathbf{D}$. The detailed formulations for calculating each coefficient Γ_{ij} are provided in Appendix B. After that, the solution of the critical static buckling load N_{scr} can be determined by solving Eq. (8).

Since the face layers in the composite sandwich plate are constructed from the isotropic solid material and the material properties are considered to be invariant, the variations of terms $\mathbf{A},\mathbf{B},\mathbf{D}$ are mainly dependent on the material properties of the core layer, and the term $\boldsymbol{\Gamma}$ is modified as:

$$\boldsymbol{\Gamma}^{\mathbf{H}}=\begin{bmatrix}\Gamma_{11}(\mathbf{C}^{\mathbf{H}}) & \Gamma_{12}(\mathbf{C}^{\mathbf{H}}) & \Gamma_{13}(\mathbf{C}^{\mathbf{H}})\\ \Gamma_{21}(\mathbf{C}^{\mathbf{H}}) & \Gamma_{22}(\mathbf{C}^{\mathbf{H}}) & \Gamma_{23}(\mathbf{C}^{\mathbf{H}})\\ \Gamma_{31}(\mathbf{C}^{\mathbf{H}}) & \Gamma_{32}(\mathbf{C}^{\mathbf{H}}) & \Gamma_{33}(\mathbf{C}^{\mathbf{H}})\end{bmatrix} \tag{10}$$

where $\boldsymbol{\Gamma}^{\mathbf{H}}$ denotes the coefficient matrix where all the coefficients in the matrix are determined by the homogenized constitutive matrix. Thus, the governing equation combining the homogenization method and FSDT for the static buckling analysis of the lattice-core composite sandwich plate with 'error-free' geometry is given via:

$$\left(\boldsymbol{\Gamma}^{\mathbf{H}}+\boldsymbol{\Lambda}\right)\boldsymbol{\Delta}=\mathbf{0} \tag{11}$$

The critical static buckling load N_{scr} calculated based on the governing equation can be functionally expressed as:

$$N_{scr}=g(E_{\mathrm{H}},G_{\mathrm{H}})=h(\mathbf{X},E_{\mathrm{B}},G_{\mathrm{B}},\rho_{\mathrm{B}}) \tag{12}$$

where E_{H} and G_{H} represent the homogenized Young's modulus and Shear modulus of the lattice material. $\mathbf{X}$ denotes the coordinates of concerned nodes in the lattice material. E_{B}, G_{B} and ρ_{B} denote the Young's modulus, Shear modulus and density of the base material to construct the lattice structure. $g(\cdot)$ denotes the physical relationship between the mesoscale material properties and N_{scr}. While $h(\cdot)$ denotes the physical relationship between the macroscale material properties and N_{scr}.

2.2. Static buckling analysis for lattice-core composite sandwich plates with AM errors

For composite sandwich plates with geometric imperfections during AM process, the AM errors should be considered as random variables in the static buckling analysis. After involving AM errors, the static buckling analysis now becomes non-deterministic with random feature. Therefore, the virtual model for this newly proposed analysis should be based on the randomness set and the random variable $\boldsymbol{\xi}^{\mathbf{R}}$ should be defined to quantify each type of AM errors including the strut node dislocation, radius variation and waviness.

Given the probability space $(\boldsymbol{\Omega},\Sigma,P)$ which is characterized by the sample space $\boldsymbol{\Omega}$, σ-algebra Σ, and the probability measure P. $\mathrm{Z}(\Re)$ denotes the set of all real random variables and $\Re$ denotes the set containing all real numbers. $\boldsymbol{\xi}^{\mathbf{R}}\in\mathrm{Z}(\Re)$ is defined as the random variable and $P_{\boldsymbol{\xi}^{\mathbf{R}}}(x)$ denotes the PDF of the random variable $\boldsymbol{\xi}^{\mathbf{R}}$.

$$\boldsymbol{\xi}^{\mathbf{R}}\in\boldsymbol{\Omega}:=\left\{\boldsymbol{\xi}^{\mathbf{R}}\in\mathrm{Z}(\Re)|\boldsymbol{\xi}^{\mathbf{R}}\sim P_{\boldsymbol{\xi}^{\mathbf{R}}}(x)\right\} \tag{13}$$

Since studies on lattice-based composite materials considering AM errors are in an early stage and relevant experimental data are still scarce, the distribution function established herein for the quantification of AM errors are mainly based on assumptions that they are following the normal distributions. When sufficient experimental data is available, more realistic distribution types can be applied in the distribution function to credibly describe the AM errors.

In the scenario of strut node dislocation, the node coordinates are defined as random variables where some of the coordinates remain to be fixed to ensure the overall structural integrity of the lattice materials. The defined nodes are shown in Fig. 3 for illustration.

In Fig. 3, the black points represent fixed nodes, and the red points represent independent random nodes. For the purpose of computational efficiency, in the octet, the orange points are defined to be dependent random nodes that are symmetrical to the random red points with respect to the virtual geometry center in green. While in vintiles, the virtual green center point is defined to be independent random nodes to control the variability, where the distance between orange dependent random nodes to the random center point is defined to be constant. The detailed statistical information of the random variables can be expressed as follows.

For the *i*-th cubic center sample:

$$\boldsymbol{\xi}^{\mathbf{R}}\in\boldsymbol{\Omega}:=\left\{x^{c}_{ij},y^{c}_{ij},z^{c}_{ij},i=1,\dots,m,j=1\right\} \tag{14}$$

For the *i*-th octet sample:

$$\boldsymbol{\xi}^{\mathbf{R}}\in\boldsymbol{\Omega}:=\left\{x^{o}_{ij},y^{o}_{ij},i=1,\dots,m,j=1,2,3\right\} \tag{15}$$

For the *i*-th vintiles sample:

$$\boldsymbol{\xi}^{\mathbf{R}}\in\boldsymbol{\Omega}:=\left\{x^{v}_{ij},y^{v}_{ij},z^{v}_{ij},i=1,\dots,m,j=1\right\} \tag{16}$$

where x_{ij},y_{ij},z_{ij} denote the x,y,z coordinates of the j-th node in the i-th lattice material sample. The superscripts c,o,v refer to the cubic center, octet, and vintiles, respectively.

In the case of radius variation, the lower quarter of struts in these lattice structures are divided into small segments of beam elements which are numbered and represented in black colour in Fig. 4. The radius of these beam elements is defined as random variables.

In Fig. 4, the red points represent the nodes that divide struts into small beam elements. In the cubic center, the red points are points of trisection, while in octets and vintiles, they are defined as points of bisection. Then, similar to the scenario of strut node dislocation, all the struts represented by the blue colour in these lattice structures are defined to be symmetrical to the lower quarter part of randomized black struts with respect to the virtual geometry center in green. Thus, the variability of the whole structure could be simulated by the defined random variables and the radius of the blue struts can be seen as the dependent variables. Followed by the elaboration and the schematic diagram, the detailed statistical information of the random variables for radius variation can be defined herein.

For the *i*-th cubic center sample:

$$\boldsymbol{\xi}^{\mathbf{R}}\in\boldsymbol{\Omega}:=\left\{r^{c}_{ij},i=1,\dots,m,j=1,2,\dots,7,8,r^{c}_{ij}>0\right\} \tag{17}$$

For the *i*-th octet sample:

$$\boldsymbol{\xi}^{\mathbf{R}}\in\boldsymbol{\Omega}:=\left\{r^{o}_{ij},i=1,\dots,m,j=1,2,\dots,8,9,r^{o}_{ij}>0\right\} \tag{18}$$

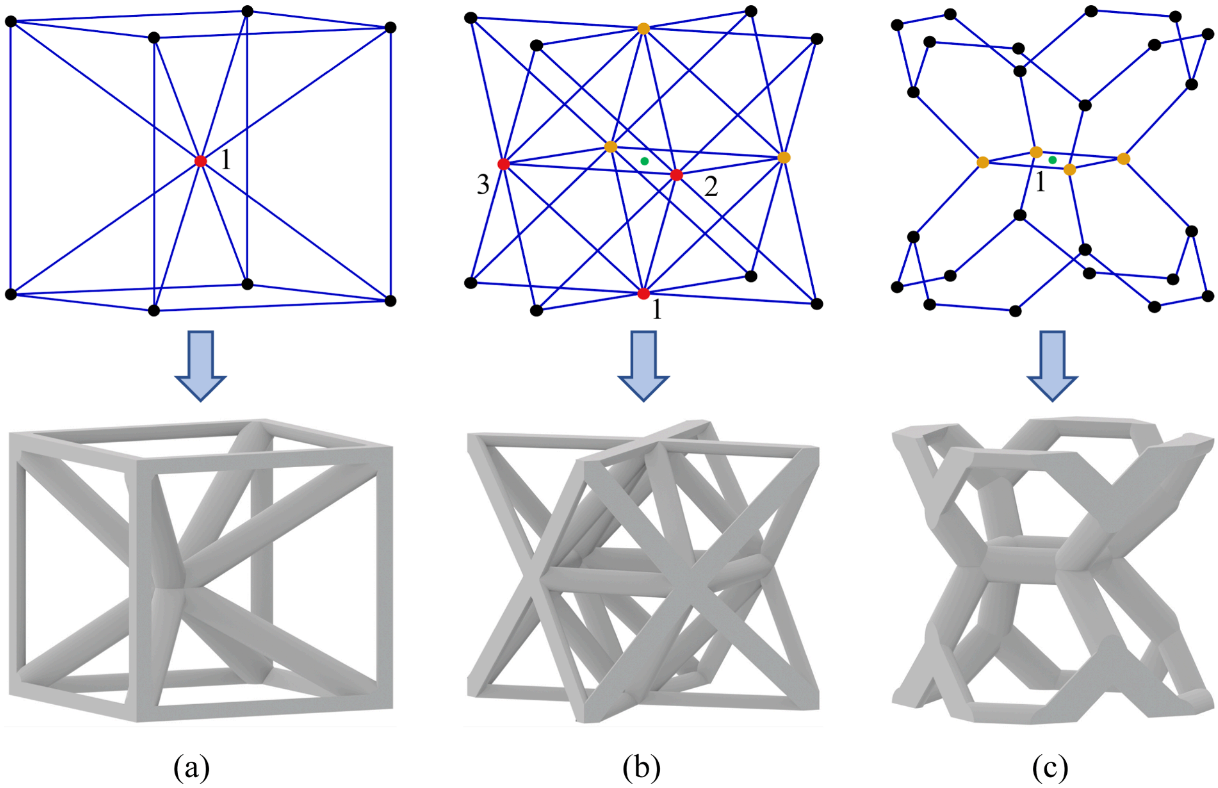

Fig. 3. Voxel models with node dislocation (a) cubic center; (b) octet; (c) vintiles.

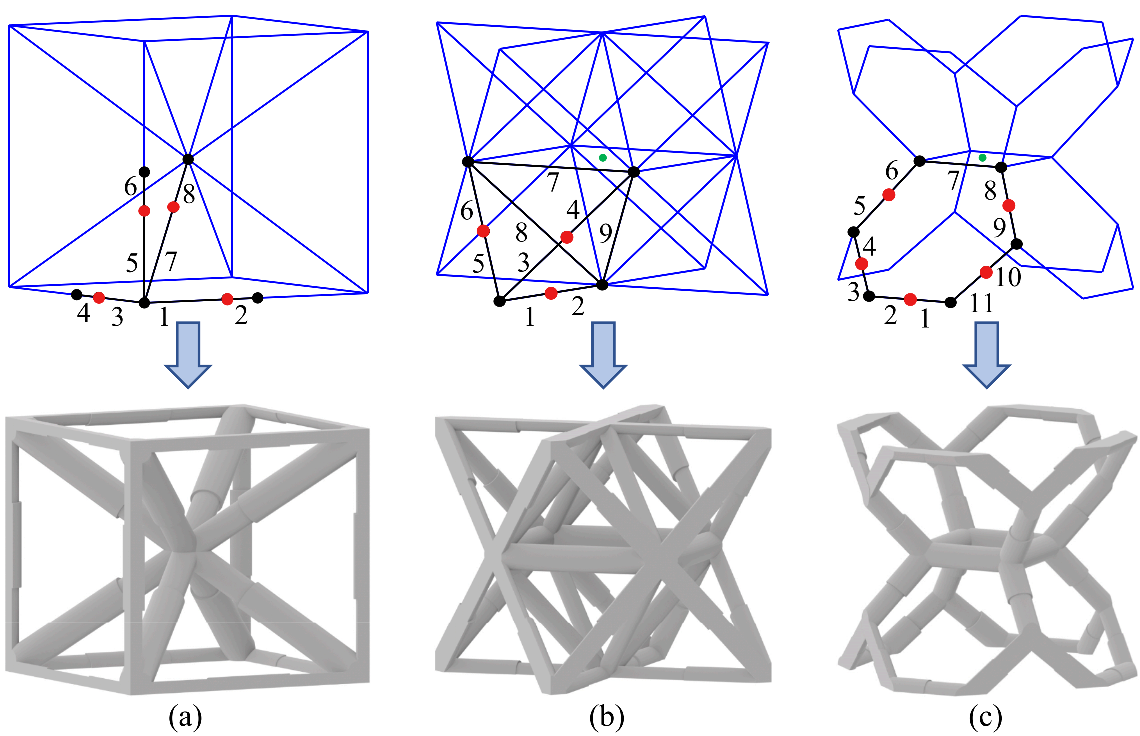

Fig. 4. Voxel models with radius variation (a) cubic center; (b) octet; (c) vintiles.

For the i-th vintiles sample:

$$\boldsymbol{\xi}^{\mathbf{R}} \in \boldsymbol{\Omega} := \left\{ r_{ij}^{v}, i = 1, \ldots, m, j = 1, 2, \ldots, 11, r_{ij}^{v} > 0 \right\} \tag{19}$$

where r_{ij} denotes the random radius of the j-th beam element in the i-th lattice material sample.

In the case of waviness, the random nodes are defined in the lower quarter part which are numbered and represented in red colour. The details are shown in Fig. 5.

In Fig. 5, the black points denote the fixed nodes, and the red points represent the random nodes where the coordinates of these points are defined as random variables. In the cubic center, the red nodes are in the

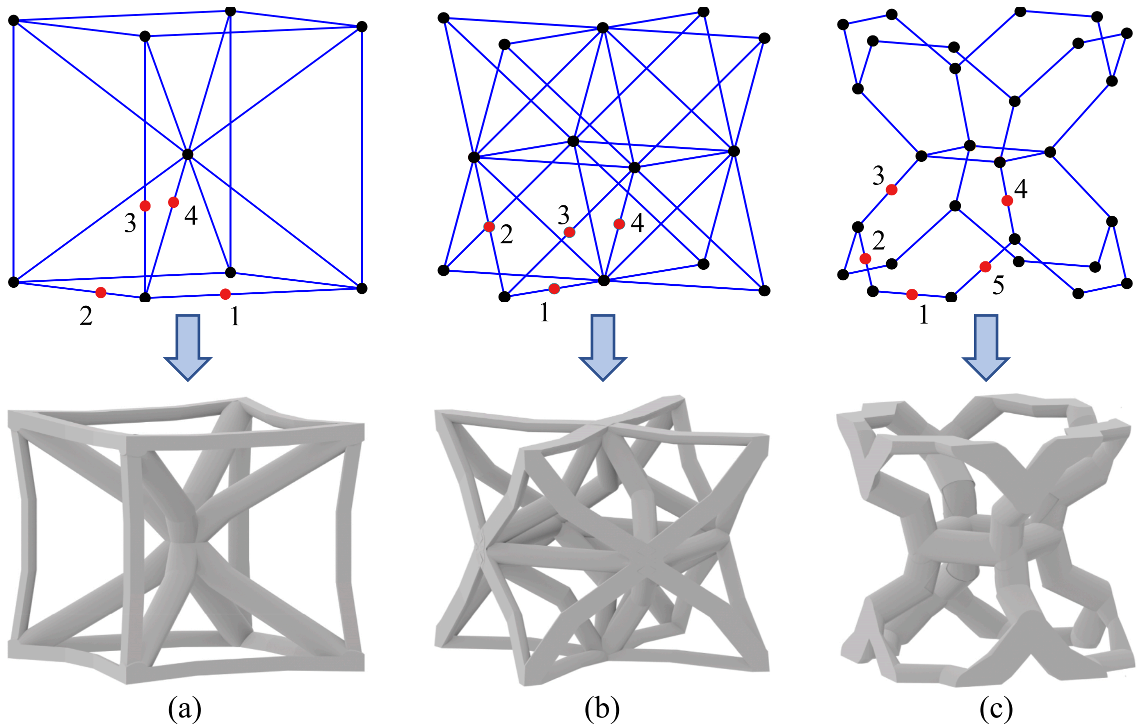

Fig. 5. Voxel models with waviness (a) cubic center; (b) octet; (c) vintiles.

position of trisection points, while in octet and vintiles, they are in the position of bisection points, which are similar to the definition in radius variation. Then the waviness of the lower quarter part of the lattice structures could be simulated. Similar to the two imperfections introduced previously, the variation of the other parts of lattice structures is defined to be symmetrical to the variation of the lower quarter part to achieve the simulation of waviness for the whole structures by using the defined random variables. Based on the explanation, the random variables can be defined as follows. The definitions of the subscripts and superscripts are the same as that in the strut node dislocation part.

For the i -th cubic center sample:

$$\boldsymbol{\xi}^{\mathbf{R}} \in \boldsymbol{\Omega} := \left\{ x_{ij}^{c}, y_{ij}^{c}, z_{ij}^{c}, i = 1, \ldots, m, j = 1, 2, 3, 4 \right\} \tag{20}$$

For the i-th octet sample:

$$\boldsymbol{\xi}^{\mathbf{R}} \in \boldsymbol{\Omega} := \left\{ x_{ij}^{o}, y_{ij}^{o}, z_{ij}^{o}, i = 1, \ldots, m, j = 1, 2, 3, 4 \right\} \tag{21}$$

For the i-th vintiles sample:

$$\boldsymbol{\xi}^{\mathbf{R}} \in \boldsymbol{\Omega} := \left\{ x_{ij}^{v}, y_{ij}^{v}, z_{ij}^{v}, i = 1, \ldots, m, j = 1, 2, 3, 4 \right\} \tag{22}$$

After the definition of the random variable $\boldsymbol{\xi}^{\mathbf{R}}$ for the three types of AM errors (i.e., strut node dislocation, radius variation, and waviness), the governing equation for the stochastic static buckling analysis of lattice-core composite sandwich plates can be updated as:

$$\left(\boldsymbol{\Gamma}^{\mathbf{H}}\left(\boldsymbol{\xi}^{\mathbf{R}}\right) + \boldsymbol{\Lambda}\left(\boldsymbol{\xi}^{\mathbf{R}}\right)\right)\boldsymbol{\Delta}\left(\boldsymbol{\xi}^{\mathbf{R}}\right) = \mathbf{0} \tag{23}$$

where the random variable $\boldsymbol{\xi}^{\mathbf{R}}$ collects all the uncertain input parameters and the terms $\boldsymbol{\Gamma}^{\mathbf{H}}\left(\boldsymbol{\xi}^{\mathbf{R}}\right)$, $\boldsymbol{\Lambda}\left(\boldsymbol{\xi}^{\mathbf{R}}\right)$ and $\boldsymbol{\Delta}\left(\boldsymbol{\xi}^{\mathbf{R}}\right)$ are dependent on $\boldsymbol{\xi}^{\mathbf{R}}$.

Since the governing equation defined in Eq. (23) involves the AM errors as random variables, the concerned response N_{scr} is considered to possess random characteristics, which could be updated as N_{scr}^{R}. The formulation in Eq. (12) which is utilized to functionally express N_{scr} can be updated as:

$$N_{scr}^{\mathrm{R}} = g\left(E_{\mathrm{H}}^{\mathrm{R}}, G_{\mathrm{H}}^{\mathrm{R}}\right) = h\left(\boldsymbol{\xi}^{\mathbf{R}}, E_{\mathrm{B}}, G_{\mathrm{B}}, \rho_{\mathrm{B}}\right) \tag{24}$$

where $E_{\mathrm{H}}^{\mathrm{R}}$ and $G_{\mathrm{H}}^{\mathrm{R}}$ denote the homogenized material properties with random feature caused by AM errors. The random variable $\boldsymbol{\xi}^{\mathbf{R}}$ denotes the quantities of AM errors. From Eq. (24), the existence of AM errors could again be proved as one of the direct consequences to influence the critical static buckling load of lattice-based structures, which is the focus of our investigation in this paper. In engineering, this relationship normally possesses underpinned and sophisticated features, which should also be expressed implicitly.

By involving manufacturing imperfections as random variables, the complexity of static buckling analysis dramatically surged. For the problem considering uncertainties, the governing equation in Eq. (24) could not be solved analytically. From the view of mathematics, it is computationally infeasible to calculate all the possible static buckling loads as there are infinite possible varieties of uncertain parameters corresponding to infinite sets of realizations for the random variables. Alternatively, the statistical characteristics can be used to describe and analyse the target buckling behaviour based on the MCS. However, although it is theoretically feasible for the stochastic analysis to acquire adequate statistical characteristics including the mean, standard deviation, PDF, and CDF, the large number of iterations would be unavoidable and significantly increase the computational costs. To address this challenge, a machine learning-aided analysis framework is established for the AM error quantification of lattice-core composite sandwich plates.

3. Static buckling analysis involving AM errors for lattice-core composite sandwich plates through X-SVR

A recently developed supervised machine learning technique, namely Extended Support Vector Regression (X-SVR) [37,38], is adopted for the static buckling analysis of lattice-core composite sandwich plates involving AM errors. To achieve a self-contained work, the algorithms of the embedded X-SVR technique are presented herein. Followed by that, the framework based on X-SVR for the quantification of the effects from AM errors is freshly introduced.

3.1. The linear X-SVR

In terms of regression, for $\mathbf{x}_i \in \Re^n (i = 1,2,...,m)$, the input and output for the training dataset are defined as:

$$\mathbf{x}_{train} = [\mathbf{x}_1, \mathbf{x}_2, ..., \mathbf{x}_i, ..., \mathbf{x}_m]^T \in \Re^{m \times n}, \mathbf{y}_{train} \in \Re^m \tag{25}$$

The targeted hyperplane for regression is defined as:

$$\widehat{f}(\mathbf{x}) = \mathbf{w}^T \mathbf{x} - \delta \tag{26}$$

where $\mathbf{w} = [w_1, w_2, ..., w_n]^T \in \Re^n$ represents the normal to the hyperplane, $\delta \in \Re$ denotes the bias and m is the number of training samples.

Considering the ε-insensitive loss function, in which ε represents the tolerable deviation between $\mathbf{y}_{train}$ and $\widehat{f}(\mathbf{x})$, the linear regression function in Eq.(26) can be solved by establishing the following optimization problem:

$$\min_{\mathbf{w},\delta,\xi,\xi^*} : \frac{1}{2}\|\mathbf{w}\|_2^2 + C\sum_{i=1}^{m}\left(\xi_i + \xi_i^*\right)$$
$$s.t.\begin{cases} \mathbf{w}^T\mathbf{x}_i - \delta - y_i \leqslant \varepsilon + \xi_i \\ y_i - \mathbf{w}^T\mathbf{x}_i + \delta \leqslant \varepsilon + \xi_i^* \\ \xi_i, \xi_i^* \geqslant 0 \end{cases} \tag{27}$$

where $C \in \Re^+ := \{x \in \Re | x > 0\}$ is the constant to determine the trade-off between the flatness of $\widehat{f}(\mathbf{x})$ and the empirical error; ξ_i and ξ_i^* represent the slack variables to denote the allowable negative and positive excessive deviations, respectively.

Since the doubly regularized support vector machine (Dr-SVM) proposed by Wang et.al [41] is an extension of the theory of support vector machine (SVM), it can be used to simultaneously conduct the classification and the feature selection process with a combination of the elastic-net penalty containing both L_1- and L_2-norm penalties. Then the governing equation for the proposed X-SVR can be expressed as follows:

$$\min_{\mathbf{p},\mathbf{q},\delta,\xi,\xi^*} : \frac{\lambda_1}{2}\left(\|\mathbf{p}\|_2^2 + \|\mathbf{q}\|_2^2\right) + \lambda_2\mathbf{e}_n^T(\mathbf{p}+\mathbf{q}) + \frac{C}{2}\left(\boldsymbol{\xi}^T\boldsymbol{\xi} + \boldsymbol{\xi}^{*T}\boldsymbol{\xi}^*\right)$$
$$s.t.\begin{cases} \mathbf{x}_{train}(\mathbf{p}-\mathbf{q}) - \delta\mathbf{e}_m - \mathbf{y}_{train} \leqslant \varepsilon\mathbf{e}_m + \boldsymbol{\xi} \\ \mathbf{y}_{train} - \mathbf{x}_{train}(\mathbf{p}-\mathbf{q}) + \delta\mathbf{e}_m \leqslant \varepsilon\mathbf{e}_m + \boldsymbol{\xi}^* \\ \mathbf{p},\mathbf{q} \geqslant \mathbf{0}_n; \boldsymbol{\xi},\boldsymbol{\xi}^* \geqslant \mathbf{0}_m \end{cases} \tag{28}$$

where $\lambda_1, \lambda_2 \in \Re^+$ indicate two tuning parameters used to balance the feature selection and classification performance; $\boldsymbol{\xi}, \boldsymbol{\xi}^* \in \Re^m$ represent two non-negative vectors for the collection of slack variables; $\mathbf{e}_n = [1, 1, ..., 1]^T \in \Re^n$ and $\mathbf{0}_n = [0, 0, ..., 0]^T \in \Re^n$, $\mathbf{p}, \mathbf{q} \in \Re^n$ consist of non-negative variables such that:

$$p_\gamma := (w_\gamma)_+ = \begin{cases} 0, w_\gamma \leqslant 0 \\ w_\gamma, w_\gamma > 0 \end{cases},$$
$$q_\gamma := (w_\gamma)_- = \begin{cases} -w_\gamma, w_\gamma < 0 \\ 0, w_\gamma \geqslant 0 \end{cases},$$
$$for\ \gamma = 1, 2, ..., n \tag{29}$$

3.2. Kernelized nonlinear X-SVR

In addition to the linear problem, the proposed X-SVR can be extended to the nonlinear regression problem. The empirical kernel mapping strategy [42] is adopted to effectively transform the linear X-SVR to a kernelized learning approach and the empirical kernelization is written as [38]:

$$\mathbf{x}_i = [x_{i,1}, x_{i,2}, ..., x_{i,n}]^T \mapsto \widehat{\kappa}(\mathbf{x}_{train}, \mathbf{x}_i) = \begin{bmatrix} \boldsymbol{\Phi}(\mathbf{x}_1)^T\boldsymbol{\Phi}(\mathbf{x}_i) \\ \boldsymbol{\Phi}(\mathbf{x}_2)^T\boldsymbol{\Phi}(\mathbf{x}_i) \\ \vdots \\ \boldsymbol{\Phi}(\mathbf{x}_m)^T\boldsymbol{\Phi}(\mathbf{x}_i) \end{bmatrix} = \begin{bmatrix} \kappa(\mathbf{x}_1, \mathbf{x}_i) \\ \kappa(\mathbf{x}_2, \mathbf{x}_i) \\ \vdots \\ \kappa(\mathbf{x}_m, \mathbf{x}_i) \end{bmatrix},$$
$$for\ i = 1, 2, ..., m \tag{30}$$

of which $\boldsymbol{\Phi}(\mathbf{x}_i)$ maps the i-th input data $\mathbf{x}_i \in \Re^n$ into a higher-dimensional Euclidian space; $\widehat{\kappa}(\mathbf{x}_i)$ denotes the i-th empirical feature vector and the empirical degree is m equalling to the number of training samples [42].

Therefore, in terms of an arbitrary training dataset $\mathbf{x}_{train} \in \Re^{m\times n}$ and a specific kernel function, the training samples can be transformed into the kernelized matrix $\boldsymbol{\kappa}_{train} \in \Re^{m\times m}$ [37]:

$$\boldsymbol{\kappa}_{train} = \begin{bmatrix} \kappa(\mathbf{x}_1, \mathbf{x}_1) & \kappa(\mathbf{x}_1, \mathbf{x}_2) & \cdots & \kappa(\mathbf{x}_1, \mathbf{x}_m) \\ \kappa(\mathbf{x}_2, \mathbf{x}_1) & \kappa(\mathbf{x}_2, \mathbf{x}_2) & \cdots & \kappa(\mathbf{x}_2, \mathbf{x}_m) \\ \vdots & \vdots & \ddots & \vdots \\ \kappa(\mathbf{x}_m, \mathbf{x}_1) & \kappa(\mathbf{x}_m, \mathbf{x}_2) & \cdots & \kappa(\mathbf{x}_m, \mathbf{x}_m) \end{bmatrix} \tag{31}$$

where the kernel matrix $\boldsymbol{\kappa}_{train}$ is adopted as the training dataset. Then the kernelized nonlinear X-SVR problem can be formulated by:

$$\min_{\widehat{\mathbf{Z}}_\kappa,\delta} : \frac{1}{2}\left(\widehat{\mathbf{Z}}_\kappa^T\widehat{\mathbf{C}}_\kappa\widehat{\mathbf{Z}}_\kappa + \delta^2\right) + \lambda_2\widehat{\mathbf{a}}_\kappa^T\widehat{\mathbf{Z}}_\kappa$$
$$s.t.\begin{cases} \boldsymbol{\kappa}_{train}(\mathbf{p}_\kappa - \mathbf{q}_\kappa) - \delta\mathbf{e}_m - \mathbf{y}_{train} \leqslant \varepsilon\mathbf{e}_m + \boldsymbol{\xi} \\ \mathbf{y}_{train} - \boldsymbol{\kappa}_{train}(\mathbf{p}_\kappa - \mathbf{q}_\kappa) + \delta\mathbf{e}_m \leqslant \varepsilon\mathbf{e}_m + \boldsymbol{\xi}^* \\ \mathbf{p}_\kappa, \mathbf{q}_\kappa, \boldsymbol{\xi}, \boldsymbol{\xi}^* \geqslant \mathbf{0}_m \end{cases} \tag{32}$$

in which the subscript κ indicates a kernelized learning model and the kernelized X-SVR is reformulated as:

$$\min_{\widehat{\mathbf{Z}}_\kappa,\delta} : \frac{1}{2}\left(\widehat{\mathbf{Z}}_\kappa^T\widehat{\mathbf{C}}_\kappa\widehat{\mathbf{Z}}_\kappa + \delta^2\right) + \lambda_2\widehat{\mathbf{a}}_\kappa^T\widehat{\mathbf{Z}}_\kappa$$
$$s.t.(\widehat{\mathbf{A}}_\kappa + \mathbf{I}_{4m\times 4m})\widehat{\mathbf{Z}}_\kappa + (\varepsilon\mathbf{I}_{4m\times 4m} + \delta\widehat{\mathbf{G}}_\kappa)\widehat{\mathbf{B}}_\kappa + \widehat{\mathbf{D}}_\kappa \geqslant \mathbf{0}_{4m} \tag{33}$$

where the kernelized matrices $\widehat{\mathbf{A}}_\kappa$, $\widehat{\mathbf{C}}_\kappa$, $\widehat{\mathbf{G}}_\kappa \in \Re^{4m\times 4m}$ are:

$$\widehat{\mathbf{A}}_\kappa = \begin{bmatrix} \mathbf{0}_{2m\times m} & \mathbf{0}_{2m\times m} & \mathbf{0}_{2m\times 2m} \\ -\kappa_{train} & \kappa_{train} & \mathbf{0}_{m\times 2m} \\ \kappa_{train} & -\kappa_{train} & \mathbf{0}_{m\times 2m} \end{bmatrix},$$
$$\widehat{\mathbf{C}}_\kappa = \begin{bmatrix} \lambda_1\mathbf{I}_{2m\times 2m} & \\ & C\mathbf{I}_{2m\times 2m} \end{bmatrix},$$
$$\widehat{\mathbf{G}}_\kappa = \begin{bmatrix} \mathbf{0}_{2m\times 2m} & \mathbf{0}_{2m\times m} & \mathbf{0}_{2m\times m} \\ \mathbf{0}_{m\times 2m} & \mathbf{I}_{m\times m} & \mathbf{0}_{m\times m} \\ \mathbf{0}_{m\times 2m} & \mathbf{0}_{m\times m} & -\mathbf{I}_{m\times m} \end{bmatrix} \tag{34}$$

The kernelized vectors $\widehat{\mathbf{a}}_\kappa, \widehat{\mathbf{B}}_\kappa, \widehat{\mathbf{D}}_\kappa, \widehat{\mathbf{Z}}_\kappa \in \Re^{4m}$ are defined as:

$$\widehat{\mathbf{a}}_\kappa = \begin{bmatrix} \mathbf{e}_{2m} \\ \mathbf{0}_{2m} \end{bmatrix}, \widehat{\mathbf{B}}_\kappa = \begin{bmatrix} \mathbf{0}_{2m} \\ \mathbf{e}_{2m} \end{bmatrix},$$
$$\widehat{\mathbf{D}}_\kappa = \begin{bmatrix} \mathbf{0}_{2m} \\ \mathbf{y}_{train} \\ -\mathbf{y}_{train} \end{bmatrix}, \widehat{\mathbf{Z}}_\kappa = \begin{bmatrix} \mathbf{p}_\kappa \\ \mathbf{q}_\kappa \\ \boldsymbol{\xi} \\ \boldsymbol{\xi}^* \end{bmatrix} \tag{35}$$

By adopting the Lagrange method with KKT conditions and introducing the non-negative Lagrange multiplier $\boldsymbol{\varphi}_\kappa \in \Re^{4m}$, the nonlinear X-SVR is calculated by a quadratic program:

$$\min_{\boldsymbol{\varphi}_\kappa} : \frac{1}{2}\boldsymbol{\varphi}_\kappa^T \mathbf{Q}_\kappa \boldsymbol{\varphi}_\kappa - \mathbf{m}_\kappa^T \boldsymbol{\varphi}_\kappa, \quad s.t.\, \boldsymbol{\varphi}_\kappa \geqslant \mathbf{0}_{4m} \tag{36}$$

where the terms $\mathbf{Q}_\kappa \in \Re^{4m\times 4m}$ and $\mathbf{m}_\kappa \in \Re^{4m}$ are defined as:

$$\begin{aligned} \mathbf{Q}_\kappa &= (\widehat{\mathbf{A}}_\kappa + \mathbf{I}_{4m\times 4m})\widehat{\mathbf{C}}_\kappa^{-1}(\widehat{\mathbf{A}}_\kappa + \mathbf{I}_{4m\times 4m})^T + \widehat{\mathbf{G}}_\kappa \widehat{\mathbf{B}}_\kappa \widehat{\mathbf{B}}_\kappa^T \widehat{\mathbf{G}}_\kappa \\ \mathbf{m}_\kappa &= \lambda_2(\widehat{\mathbf{A}}_\kappa + \mathbf{I}_{4m\times 4m})\widehat{\mathbf{C}}_\kappa^{-1}\widehat{\mathbf{a}}_\kappa - \varepsilon \widehat{\mathbf{B}}_\kappa - \widehat{\mathbf{D}}_\kappa \end{aligned} \tag{37}$$

Considering $\boldsymbol{\varphi}_\kappa^* \in \Re^{4m}$ as the solution of Eq.(36), the variables $\widehat{\mathbf{Z}}_\kappa, \boldsymbol{\delta}_\kappa$ are formulated as:

$$\begin{aligned} \widehat{\mathbf{Z}}_\kappa &= \widehat{\mathbf{C}}_\kappa^{-1}\left[(\widehat{\mathbf{A}}_\kappa + \mathbf{I}_{4m\times 4m})^T \boldsymbol{\varphi}_\kappa^* - \lambda_2 \widehat{\mathbf{a}}_\kappa\right], \\ \boldsymbol{\delta}_\kappa &= \widehat{\mathbf{B}}_\kappa^T \widehat{\mathbf{G}}_\kappa \boldsymbol{\varphi}_\kappa^* \end{aligned} \tag{38}$$

The nonlinear regression function obtained by the kernelized X-SVR can be obtained as:

$$\widehat{f}_\kappa(\mathbf{x}) = (\mathbf{p}_\kappa - \mathbf{q}_\kappa)^T \boldsymbol{\kappa}(\mathbf{x}_{train}, \mathbf{x}) - \widehat{\mathbf{B}}_\kappa^T \widehat{\mathbf{G}}_\kappa \boldsymbol{\varphi}_\kappa^* \tag{39}$$

where $\boldsymbol{\kappa}(\mathbf{x}_{train}, \mathbf{x}) \in \Re^m$ denotes the kernelized input matrix.

3.3. Machine learning-aided stochastic static buckling analysis for composite sandwich plates

For the illustration of quantifying the effects of AM error on the static buckling behaviour of lattice-core composite sandwich plates, the detailed steps for the proposed methodology combining static buckling analysis with the kernelized X-SVR technique are introduced herein.

Step 1 Generate m samples of lattice-core composite sandwich plates with random variables for the three types of manufacturing imperfections (i.e., strut node dislocation, radius variation, and waviness). Define m as the size of the training dataset, n as the dimension of the random variables, and $\mathbf{x}_i$ as the i-th lattice material sample, then the training dataset $\mathbf{x}_{train}$ can be represented as:

$$\mathbf{x}_{train} := \{\mathbf{x}_i \in \Re^n, for\, i = 1, ..., m\}, \mathbf{x}_{train} \in \Re^{m\times n} \tag{40}$$

Step 2 Construct the voxel models for the lattice materials in the training dataset based on the information provided in each $\mathbf{x}_i$ and calculate the homogenized constitutive matrix to get Young's modulus, shear modulus, and Poisson's ratio using the numerical homogenization method given in Section 2.1.

Step 3 Determine the critical static buckling load for the lattice-core composite sandwich plate which is constructed from the i-th lattice material sample in the training dataset based on FSDT mentioned in Section 2.1; define $\mathbf{y}_{train}$ as the output of the training dataset:

$$\mathbf{y}_{train} := \left\{y_i = N_{scr}^i, for\, i = 1, ..., m\right\}, \mathbf{y}_{train} \in \Re^m \tag{41}$$

Step 4 Establish a regression model by utilizing the generated training dataset with the kernelized X-SVR regression model:

$$\widehat{f}_\kappa(\mathbf{x}) = (\mathbf{p}_\kappa - \mathbf{q}_\kappa)^T \boldsymbol{\kappa}(\mathbf{x}_{train}, \mathbf{x}) - \widehat{\mathbf{B}}_\kappa^T \widehat{\mathbf{G}}_\kappa \boldsymbol{\varphi}_\kappa^* \tag{42}$$

Step 5 Generate new inputs that follow the statistical models of AM errors. Herein, due to the insufficiency of the experimental data, the statistical models of AM errors are mainly based on assumptions that they are following normal distributions.

Step 6 By importing the new inputs $\mathbf{x}_{new}$ into the established virtual model, calculate the corresponding buckling load N_{scr} according to $\widehat{f}_\kappa(\mathbf{x})$ and implement the sampling method.

Step 7 Generate the statistical properties including the mean, standard deviation, PDF and CDF based on N_{scr}.

Based on the elaboration, the newly proposed framework is capable of quantifying the effects of AM errors on the static buckling behaviour of lattice-core composite sandwich plates by utilizing the recently developed kernelized X-SVR. The novelties and advantages possessed within the present work could be summarized into the following aspects: wide applicability, unrestricted selection, high compatibility, computational efficiency, and adequate statistical information. In terms of applicability, the proposed framework supports various types of lattice-core composite structures including cubic center, octet, vintiles, etc., in which multiple AM errors induced during the manufacturing process can be targeted, including strut node dislocation, radius variation, waviness, etc. The feature of wide applicability could enable the developed methodology to analyse a diverse array of lattice-based composite structures with unique design and complex internal structures. For unrestricted selection, the quantities of interest for both inputs and outputs within the system are not confined to a single type of distribution. The AM errors within the framework could be quantified into various appropriate statistical moments and distribution types. Therefore, the random variables for quantifying the AM errors can be defined based on the statistical information from industries or experiments, which could be imported correspondingly into the proposed virtual model. Besides, the integration of machine learning techniques including clustering strategy, normalization, feature selection, etc., could enhance the compatibility of the proposed framework, improve the performance of the developed model, and ensure the model robustness when the input data varies. In addition, employing the sampling-based method to express the established virtual model as an explicit formulation could significantly enhance the computational efficiency, which could contribute to the reduction in computational time compared to traditional MCS. The implementation of sampling-based method could also enable the effective collection of a comprehensive set of statistical information related to any concerned structural response, including the means, standard deviations, PDF and CDF. Furthermore, the proposed virtual model-aided AM error quantification strategy possesses other inherent features such as the feasibility of information update, hypothesis analysis, sensitivity analysis, etc., all of which can be implemented on the established virtual model in a computationally efficient manner. We believe that the proposed strategy for the quantification of AM errors could provide engineers a viable access to investigate the sophisticated mechanisms from the manufacturing imperfections in micro or meso-scale to the overall structural performance in macroscale, which could convincingly verify its potential in advanced manufacturing and composite engineering.

4. Numerical investigation

To demonstrate the applicability of the proposed machine learning-aided stochastic analysis framework, the numerical examples for cubic center, octet, and vintiles based composite sandwich plates considering AM errors, including strut node dislocation, radius variation, and waviness, are thoroughly investigated, where the number of samples in the dataset for each lattice form is set as 5000. The statistical information which covers the mean, standard deviation, PDF, and CDF are subsequently provided for quantifying the effects of these errors. Moreover, the inherent feature of information update for the proposed methodology is given after the numerical examples. All the investigations are conducted by DELL 7920 Tower with Intel Xeon Gold 5215 CPU @ 2.50 *GHz* and 128 *GB* of RAM.

4.1. Numerical validation

Before conducting the numerical investigation, the accuracy and efficiency of the X-SVR analysis framework should be studied and verified. Firstly, the comparison between the proposed methodology and the other commonly applied machine learning techniques (Gaussian Process Regression (GPR), Support Vector Machine (SVR), Decision Tree (DT), and Neural Network (NN)) is performed for strut node dislocation, radius variation, and waviness, respectively. The convergence study of estimated R^2 values is given in Fig. 6. It can be observed that the performance of the proposed X-SVR model is more accurate and robust than

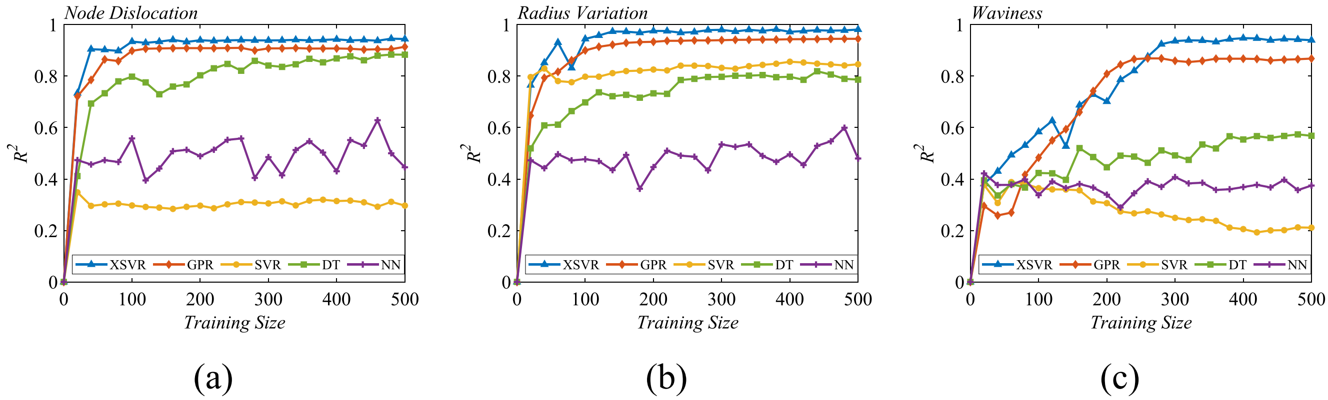

Fig. 6. Convergence study of different machine learning models for (a) strut node dislocation; (b) radius variation; (c) waviness.

the other machine learning models, as evidenced by a relatively higher convergence rate and the highest R^2 value. Based on the plot of the convergence study, the size of the training dataset is taken as $m = 500$ for strut node dislocation, radius variation, and waviness.

To estimate the computational accuracy, the R^2 and *NRMSE* are selected as the estimation indices [37]. Based on the convergence study, the X-SVR model is trained with 500 samples and Table 1 gives the values of R^2, *NRMSE* and the computational time of the corresponding trained models under simply supported (SSSS) and clamped boundary conditions (CCCC) for the target composite plates. From Table 1, it can be seen that the values of R^2 are all greater than 0.9 and those of *NRMSE* are nearly 0, suggesting the great accuracy and robustness of the embedded X-SVR technique in generating virtual models by considering different boundary conditions and AM error types.

In terms of computational time, the left column shows the estimated time required for training the X-SVR model using the existing 500 training samples plus the time required for calculating the static buckling load of 5000 new samples, and the right column shows the estimated time for calculating the static buckling load of 5000 new samples by utilizing the MCS. The imperfection type of node dislocation, radius variation and waviness under both simply supported and clamped boundary condition are recorded, respectively. For node dislocation, the computational time is around 6.7 and 6.3 min for the X-SVR regression model, demonstrating a dramatic reduction compared to 5600 min required by MCS. In terms of radius variation, the X-SVR regression model requires about 7.1 min' computational time, a decrease of more than 1000 times compared to the time needed for MCS. In the case of waviness, the recorded time is about 6.8 min and 7.7 min for X-SVR while MCS requires 7700 min. The computational time again significantly decreases for both boundary conditions. Thus, the results could indicate remarkable improvements for all the imperfection types and boundary conditions in computational efficiency when using the X-SVR regression model compared to the traditional MCS method.

4.2. Numerical results and discussion

The statistical information of the random variables used to define and mimic the AM error is given in Table 2. The parameter d and the subscript (o) denote the strut diameter and original. The definition for the rest variables could be found in Section 2.2.

Three aforementioned lattice materials with 10 % relative density ($\rho^* = 10\%$) for the core layer are investigated under both simply supported and clamped boundary conditions. The geometrical information of the composite sandwich plate is taken as: $L_a = L_b = 1\,m$, $h = 5cm, R_{hc} = h_c/h = 0.98$. The base material properties of the face layer and the core layer, and the homogenized material properties for the lattice core are detailed in Tables 3 and 4.

The static buckling loads of lattice-core composite sandwich plates with 'error-free' geometry are calculated in Table 5. It can be seen that a higher static buckling load is expected under the clamped boundary condition, which can be explained by the extra constraints provided on the plate edges. Among the three lattice types, the octet lattice material shows the highest static buckling capacity under both boundary conditions.

Table 1
Estimation metrics of the virtual models.

Imperfection type	Boundary condition	R^2	*NRMSE*	Computational time (mins)	
				X-SVR	MCS
Node Dislocation	SSSS	0.9423	0.0007382	6.7893	5656.8927
	CCCC	0.9355	0.0006202	6.3443	5634.2137
Radius Variation	SSSS	0.9996	0.0035102	7.1875	8568.8880
	CCCC	0.9814	0.0030944	7.1298	8571.1107
Waviness	SSSS	0.9514	0.0049302	6.8032	7733.9452
	CCCC	0.9169	0.0055493	7.7785	7729.8725

Table 2
Statistical information of the considered random variables for AM errors.

AM error	Random variables	Distribution type	Mean	Std
Node dislocation	x_{ij}, y_{ij}, z_{ij}	Normal	$x_{ij(o)}, y_{ij(o)}, z_{ij(o)}$	$0.5d_{(o)}$
Radius variation	r_{ij}	Normal	$r_{(o)}$	$0.25d_{(o)}$
Waviness	x_{ij}, y_{ij}, z_{ij}	Normal	$x_{ij(o)}, y_{ij(o)}, z_{ij(o)}$	$0.25d_{(o)}$

Table 3
Base material properties for the composite sandwich plate.

	Material type	E(GPa)	ν	$\rho(\mathrm{kg/m^3})$
Face layer	Al	68.3	0.34	2689.8
Core layer	Ti-6Al-4V	110	0.34	4450

Table 4
Effective material properties for different types of lattice-core.

Lattice material	E(GPa)	ν	G(GPa)
Cubic center	2.0488	0.2795	0.9018
Octet	1.7345	0.3346	1.1932
Vintiles	1.2856	0.3780	0.2949

Table 5
Static buckling loads (N) for the 'error-free' composite sandwich plate with different lattice cores.

Relative density	Lattice type	Simply supported	Clamped
10 %	Cubic center	2,829,665	7,206,027
	Octet	2,909,635	7,234,839
	Vintiles	2,400,967	6,119,772

4.2.1. Strut node dislocation

The statistical plots including the PDFs and CDFs for the static buckling behaviour of the cubic center lattice-core composite sandwich plate with strut node dislocation are illustrated in Fig. 7, where the results from the X-SVR regression model are drawn against those based on the MCS to validate the applicability of the proposed method. We may find out that the proposed methodology is competent to deliver adequate estimations by utilizing 500 training samples in this case. Apart from the PDFs and CDFs, the accuracy of the proposed framework has been further verified by comparing the calculated probabilities, the mean value and the standard deviation between the X-SVR and MCS

Table 6
Comparison of estimated probability for N_{scr} between X-SVR and MCS for cubic center core composite sandwich plate.

Probability	MCS (SSSS)	X-SVR (SSSS)	MCS (CCCC)	X-SVR (CCCC)
$P(N_{scr} \leq \mu - 3\sigma)$	0.017307	0.017667	0.015459	0.016185
$P(N_{scr} \leq \mu - 2\sigma)$	0.045950	0.046440	0.046129	0.046966
$P(N_{scr} \leq \mu - \sigma)$	0.130364	0.133765	0.137772	0.139411
$P(N_{scr} \leq \mu)$	0.395841	0.389659	0.401796	0.392273
$P(N_{scr} \leq \mu + \sigma)$	0.900304	0.901484	0.900131	0.902657
$P(N_{scr} \leq \mu + 2\sigma)$	0.999760	0.999831	0.999751	0.999821
$P(N_{scr} \leq \mu + 3\sigma)$	1.000000	1.000000	1.000000	1.000000
$P(N_{scr} \leq N_{scr(o)})$	0.000499	0.000487	0.000414	0.000396
μ(N)	2901889.40	2901961.88	7359992.28	7360229.40
σ(N)	10970.81	10846.64	22929.53	22794.77
σ/μ	0.003781	0.003737	0.003115	0.003097

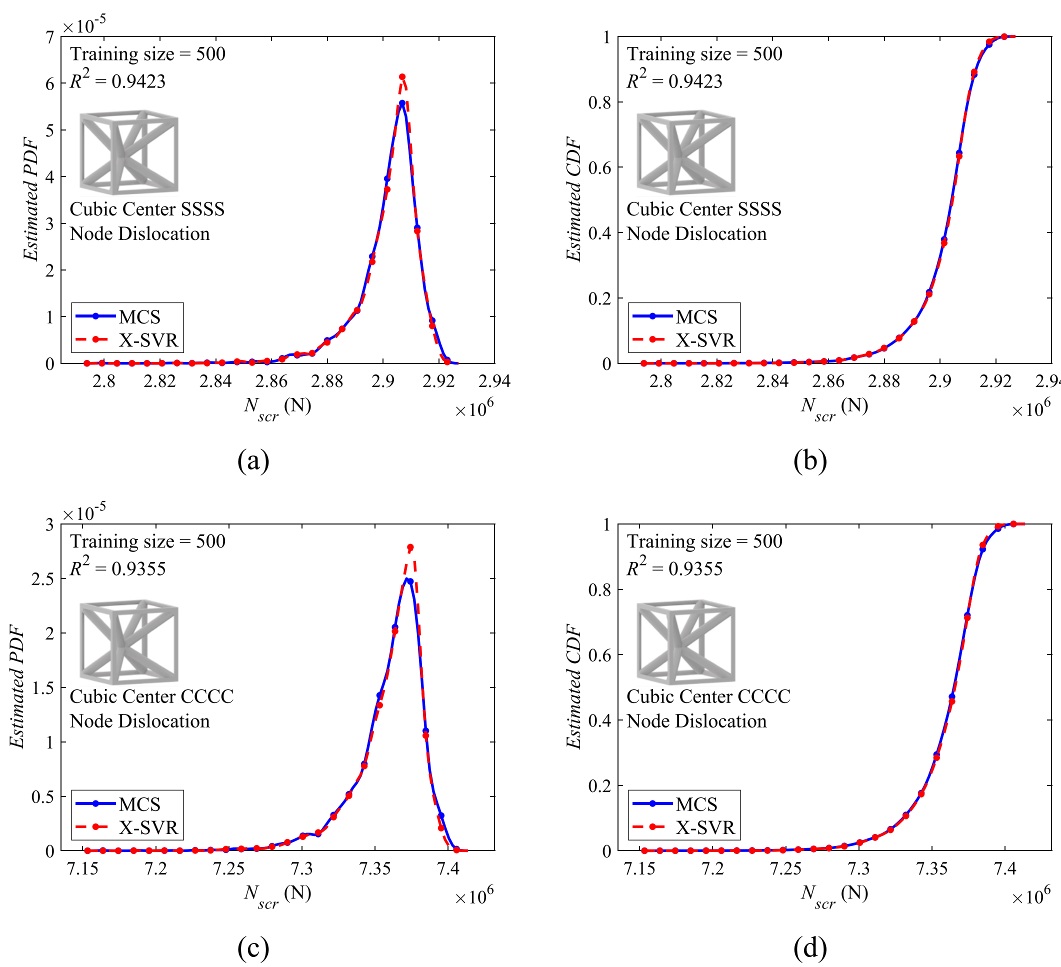

Fig. 7. Estimated strut node dislocation statistical results: (a) PDF for the simply supported composite sandwich plate with cubic center lattice-core; (b) CDF for the simply supported composite sandwich plate with cubic center lattice-core; (c) PDF for the clamped composite sandwich plate with cubic center lattice-core; (d) CDF for the clamped composite sandwich plate with cubic center lattice-core.

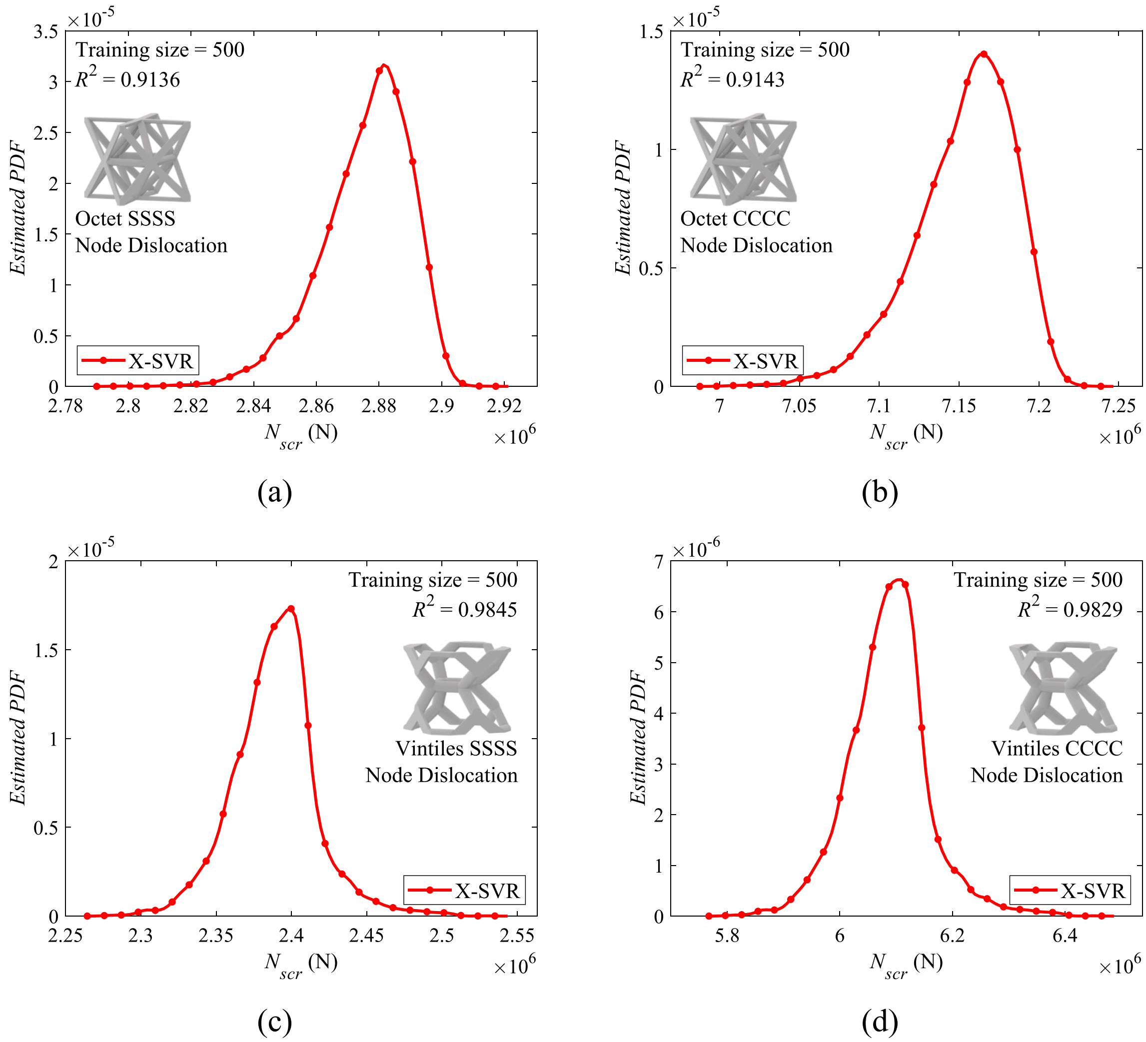

Fig. 8. Estimated strut node dislocation statistical results: (a) PDF for the simply supported composite sandwich plate with octet lattice-core; (b) PDF for the clamped composite sandwich plate with octet lattice-core; (c) PDF for the simply supported composite sandwich plate with vintiles lattice-core; (d) PDF for the clamped composite sandwich plate with vintiles lattice-core.

approaches, as shown in Table 6 ($N_{scr(o)}$ denotes the original static buckling load).

From Table 6, it is evident that the estimated probabilities calculated based on the X-SVR model match well with the MCS simulation regardless of the locations ranging from $\mu - 3\sigma$ to $\mu + 3\sigma$. In addition, the $P(N_{scr} \leqslant N_{scr(o)})$, the mean value $\mu(N)$ and the standard deviation $\sigma(N)$ of the static buckling load agree well between the two methods. According to $P(N_{scr} \leqslant N_{scr(o)}) \approx (4 \sim 5) \times 10^{-4}$, the strut node dislocation would potentially increase the overall static buckling load of the cubic center core composite sandwich plate under both simply supported and clamped boundary conditions. The small ratio between σ and μ suggests the possible values of static buckling load tend to be close to the mean.

Followed by the comparison between the proposed X-SVR framework and MCS, similar statistical investigations on octet and vintiles core composite sandwich plates are conducted in Fig. 8. Then the calculation results under both simply supported and clamped boundary conditions are presented in Table 7 including the probabilities, the estimated mean values, and the standard deviation.

Based on Fig. 8, considering the variation of boundary conditions only, a similar pattern of PDF could be observed for both types of lattice-core, while comparing the PDF between the two types of composite sandwich plate, an different shape could be observed for the one with octet lattice-core, which indicates that under the same type of AM error, the influence of the lattice-core internal structure is more evident than that of the boundary conditions on the static buckling behaviour. Besides, by observing the x-axis in the PDF plots, the values of static buckling load are generally higher in the octet core composite sandwich plate compared with that in the vintiles core composite sandwich plate

Table 7
Estimated probability of N_{scr} for the octet core and vintiles core composite sandwich plate using the X-SVR method.

Probability	Octet (SSSS)	Octet (CCCC)	Vintiles (SSSS)	Vintiles (CCCC)
$P(N_{scr} \leq \mu - 3\sigma)$	0.008442	0.009170	0.004133	0.003885
$P(N_{scr} \leq \mu - 2\sigma)$	0.043826	0.041984	0.027613	0.026210
$P(N_{scr} \leq \mu - \sigma)$	0.157350	0.158399	0.144599	0.142795
$P(N_{scr} \leq \mu)$	0.441142	0.442184	0.484781	0.489392
$P(N_{scr} \leq \mu + \sigma)$	0.847525	0.846048	0.885250	0.883756
$P(N_{scr} \leq \mu + 2\sigma)$	0.997720	0.997479	0.968861	0.967783
$P(N_{scr} \leq \mu + 3\sigma)$	0.999993	0.999999	0.990335	0.990024
$P(N_{scr} \leq N_{scr(o)})$	0.999742	0.999962	0.689764	0.710188
μ(N)	2875833.17	7153481.31	2388881.27	6086224.65
σ(N)	14080.00	30813.71	27800.66	72051.58
σ/μ	0.004896	0.004308	0.011638	0.011838

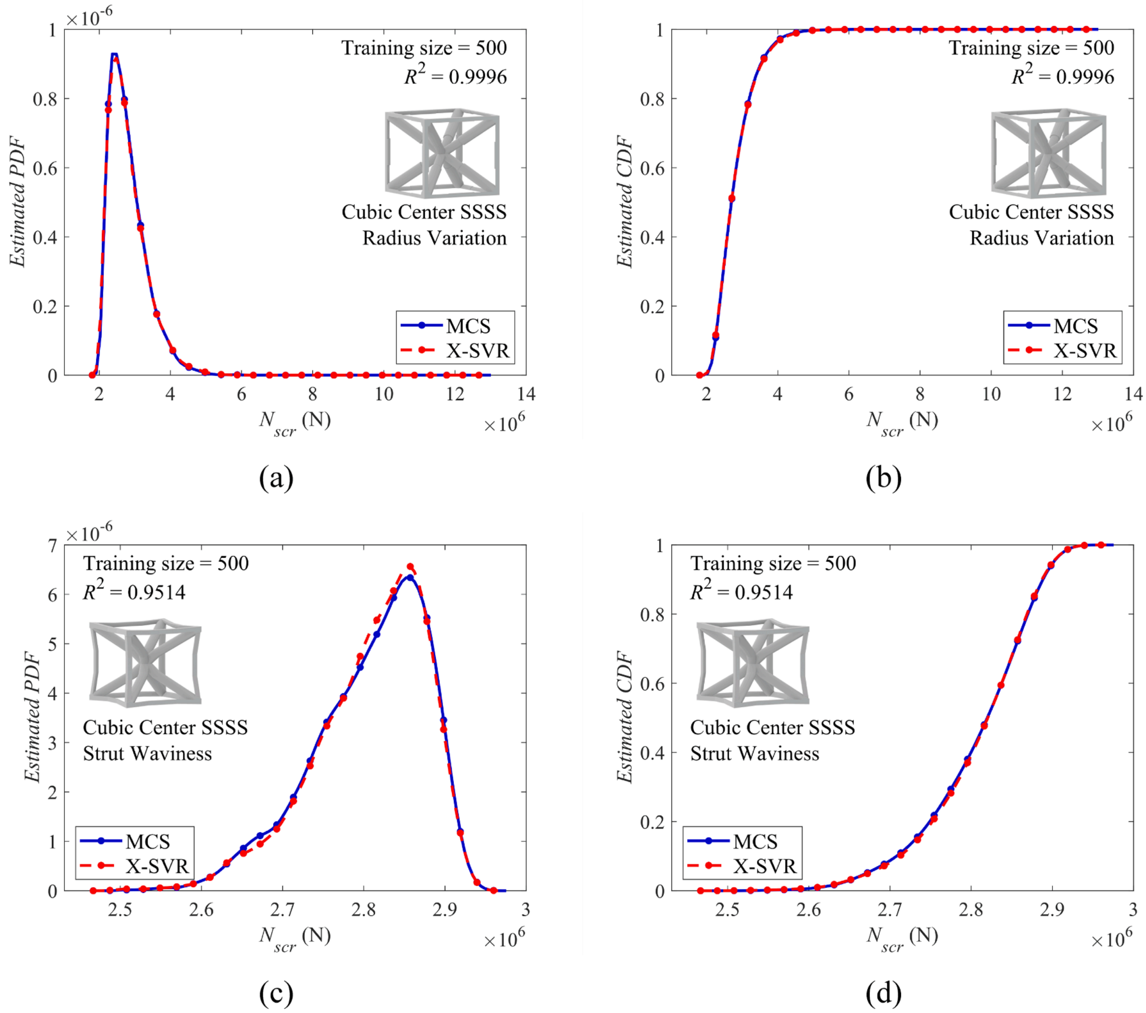

Fig. 9. Estimated statistical results for the simply supported composite sandwich plate with cubic center lattice-core: (a) PDF for radius variation; (b) CDF for radius variation; (c) PDF for waviness; (d) CDF for waviness.

under both boundary conditions. In addition, by comparing the calculation results in Table 7, it can be seen that for the same composite sandwich plate with different boundary conditions, the values of probabilities for the selected locations agree well. While for the composite sandwich plate with a different lattice-core and the same boundary condition, the differences between the probability values are comparatively larger, which further demonstrates the greater influence of the lattice-core internal structure rather than the boundary conditions. Furthermore, in terms of the probabilities for $N_{scr} \leqslant N_{scr(o)}$, the composite sandwich plate with octet core layer and vintiles core layer reach around 99.9 % and 70 % respectively, meaning that the strut node dislocation would weaken the static buckling load capacity for most composite sandwich plates with these two types of lattice-core layer.

4.2.2. Radius variation and waviness

The statistical plots for the cubic center core composite sandwich plate under the simply supported boundary condition are provided in Fig. 9 for the AM error of radius variation and waviness respectively, where the estimated PDFs and CDFs computed by the X-SVR framework are compared with that computed by the MCS to illustrate the capability and accuracy of the proposed methodology for the stochastic static buckling analysis considering the two manufacturing imperfections above.

Based on the plots in Fig. 9, the proposed X-SVR model shows great capability and competency to estimate the static buckling behaviour of the lattice-core composite sandwich plate under the AM error of radius variation and waviness, where the statistical plots computed from the X-SVR model match well with those via the MCS simulation. The values of R^2, which are given as 0.9996 and 0.9514 for the radius variation and waviness respectively, further indicate the great accuracy of the proposed methodology. In addition to the PDFs and CDFs, the computed probability, the mean value, and the standard deviation calculated via X-SVR and MCS are shown in Table 8.

Table 8
Estimated probability of N_{scr} for the simply supported cubic center core composite sandwich plate with radius variation and waviness.

Probability	Radius variation		Waviness	
	MCS	X-SVR	MCS	X-SVR
$P(N_{scr} \leq \mu - 3\sigma)$	0.000000	0.000000	0.006213	0.006692
$P(N_{scr} \leq \mu - 2\sigma)$	0.000007	0.000009	0.047433	0.047518
$P(N_{scr} \leq \mu - \sigma)$	0.124155	0.125030	0.165991	0.162001
$P(N_{scr} \leq \mu)$	0.583363	0.585491	0.436126	0.433692
$P(N_{scr} \leq \mu + \sigma)$	0.853149	0.850100	0.842640	0.849542
$P(N_{scr} \leq \mu + 2\sigma)$	0.955938	0.952964	0.999652	0.999620
$P(N_{scr} \leq \mu + 3\sigma)$	0.988191	0.986547	1.000000	1.000000
$P(N_{scr} \leq N_{scr(o)})$	0.600090	0.601553	0.553863	0.553101
μ(N)	2806029.04	2806713.50	2807329.11	2808161.83
σ(N)	532461.89	533446.53	69723.53	69534.13
σ/μ	0.189756	0.190006	0.024836	0.024761

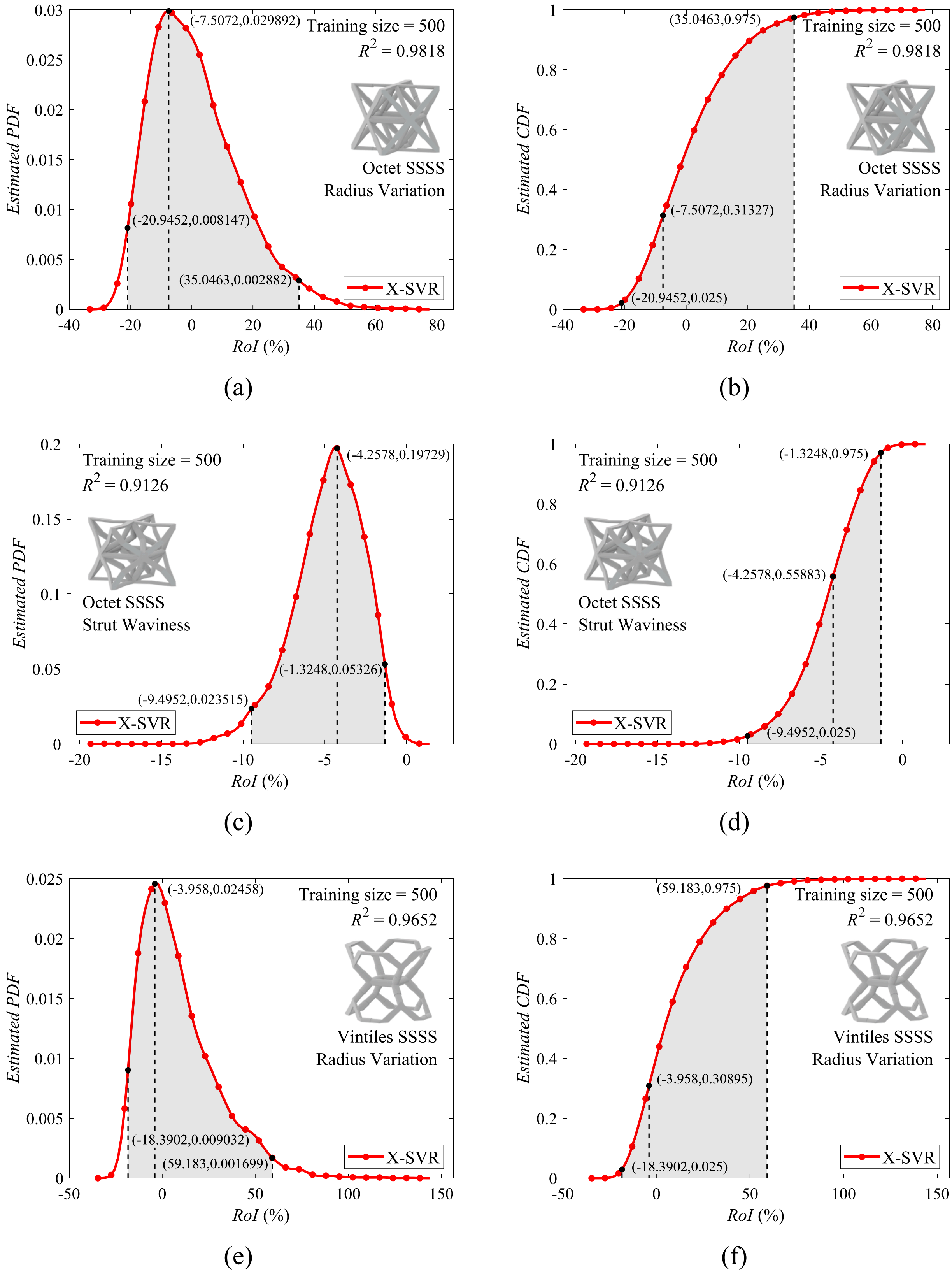

Fig. 10. The estimated ratio of interval for the simply supported composite sandwich plate: (a) PDF for radius variation octet; (b) CDF for radius variation octet; (c) PDF for waviness octet; (d) CDF for waviness octet; (e) PDF for radius variation vintiles; (f) CDF for radius variation vintiles; (g) PDF for waviness vintiles; (h) CDF for waviness vintiles.

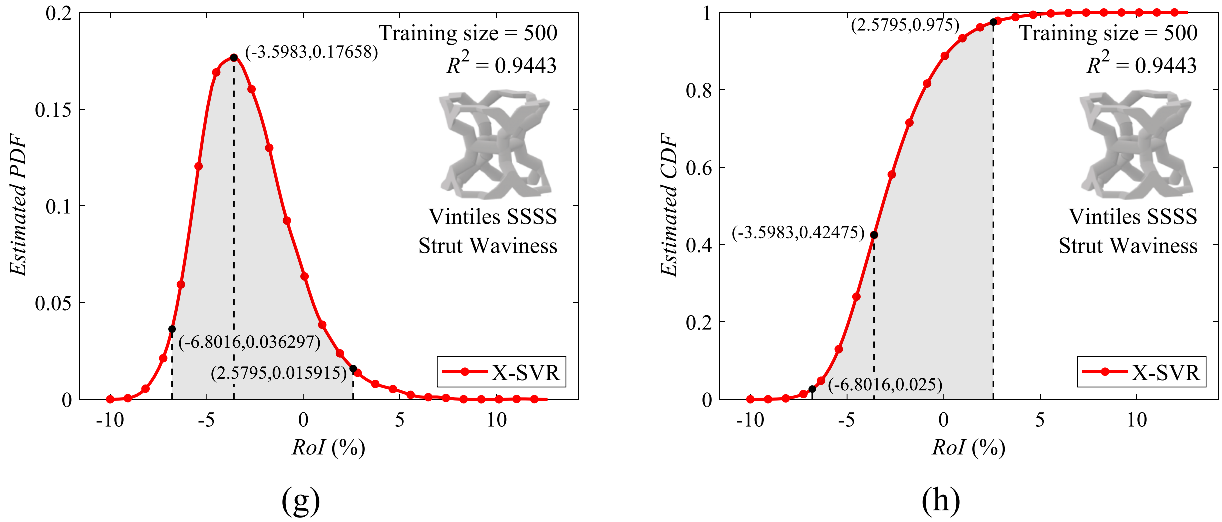

Fig. 10. (*continued*).

Table 9
Estimated probabilities of *RoI* for the simply supported composite sandwich plate with radius variation and waviness.

Probability	Octet		Vintiles	
	Radius Variation	Waviness	Radius Variation	Waviness
$P(RoI \le 0)$	0.529229	0.998733	0.405481	0.883522
$\mu(RoI)(\%)$	1.142639	−4.758660	8.708664	−2.895942
$\sigma(RoI)(\%)$	14.251814	2.102499	20.365245	2.361989

It is evident that the proposed X-SVR approach is competent to provide accurate estimation. The probabilities of $N_{scr} \leqslant N_{scr(o)}$ for radius variation and waviness are estimated to be around 60 % and 55 %, respectively. This indicates that the two types of manufacturing imperfections could potentially weaken the plate and the chance from radius variation is larger.

Followed by the investigation of the cubic center core composite sandwich plate under the two types of manufacturing imperfections, the percentage change of the static buckling load under the simply supported boundary condition is plotted in terms of PDFs and CDFs for the radius variation and waviness in Fig. 10. Then the study of the static buckling behaviour of the octet core and vintiles core composite sandwich plate could be conducted. A new parameter: ratio of interval (*RoI*) used in the following part is defined herein.

$$RoI = \frac{N_{scr} - N_{scr(o)}}{N_{scr(o)}} \times 100\% \tag{43}$$

In the PDF and CDF plots from Fig. 10, the grey shadow represents the range of 95% confidence interval. By comparing the values of *RoI* in the figure, a wider range could be observed in the case of radius variation for both types of composite plates, which means that the influence of radius variation is considered to be greater than that of waviness. Besides, the highest probabilities are indicated in the plots. For the octet core composite sandwich plate, the values are 0.029892 and 0.197290 under radius variation and waviness, respectively. When considering the vintiles core composite sandwich plate, the values are 0.024580 and 0.176580. Based on the values above, the highest probabilities in octet core composite sandwich plate are comparatively larger under both types of imperfections. After that, the estimated probabilities for $RoI \leqslant 0$, $\mu(RoI)$ and $\sigma(RoI)$ are provided in Table 9.

Based on the values of $P(RoI \leqslant 0)$, the effects of waviness which causes the decrease of static buckling load can be greater than that caused by radius variation for both types of composite sandwich plates. By comparing the standard deviations of *RoI*, greater values can be observed in the case of radius variation for both types of composite plates. This again indicates that the range of static buckling load change caused by radius variation is greater than that caused by waviness where the distributions are separated further apart with respect to the mean values.

4.2.3. Information update for the X-SVR analysis framework

To ensure the adjusted statistical models could be integrated and applied into the proposed analysis framework, the inherent feature of unrestricted selection and information update for the random variables should be validated in this section. The cubic center core composite sandwich plate with the AM error of radius variation is selected as the investigating numerical example and various appropriate distribution types are utilized to quantify the AM errors. Three different statistical distribution including the uniform distribution, gamma distribution, and beta distribution are selected to define the radius variation of horizontal strut, vertical strut, and diagonal strut in the cubic center lattice-core, respectively. The detailed statistical information of the random variables is defined in Table 10.

To demonstrate the applicability and accuracy of information update for the proposed machine learning-aided framework, the PDF and CDF for the static buckling behaviour considering the above three distributions together are given in Fig. 11, where the plots are compared against that computed by the MCS. Followed by that, the estimated probabilities, the mean value, and the standard deviation calculated from the trained X-SVR model and MCS are presented in Table 11.

Based on the statistical plot, it could be observed that the PDF and CDF curves computed by the previously trained X-SVR model overlap with that computed from the MCS. The well-matched curves indicate the high accuracy of the proposed machine learning-aided training model, which could demonstrate the inherent feature of information update for the proposed analysis framework. Besides, by comparing the probabil-

Table 10
Statistical information for cubic center lattice-core composite sandwich plate under the defects of radius variation.

Property	Distribution type	Mean (cm)	Standard deviation (cm)
Radius variation for horizontal strut	Uniform	0.0604	0.0313
Radius variation for vertical strut	Gamma	0.0442	0.0161
Radius variation for diagonal strut	Beta	0.0353	0.0163

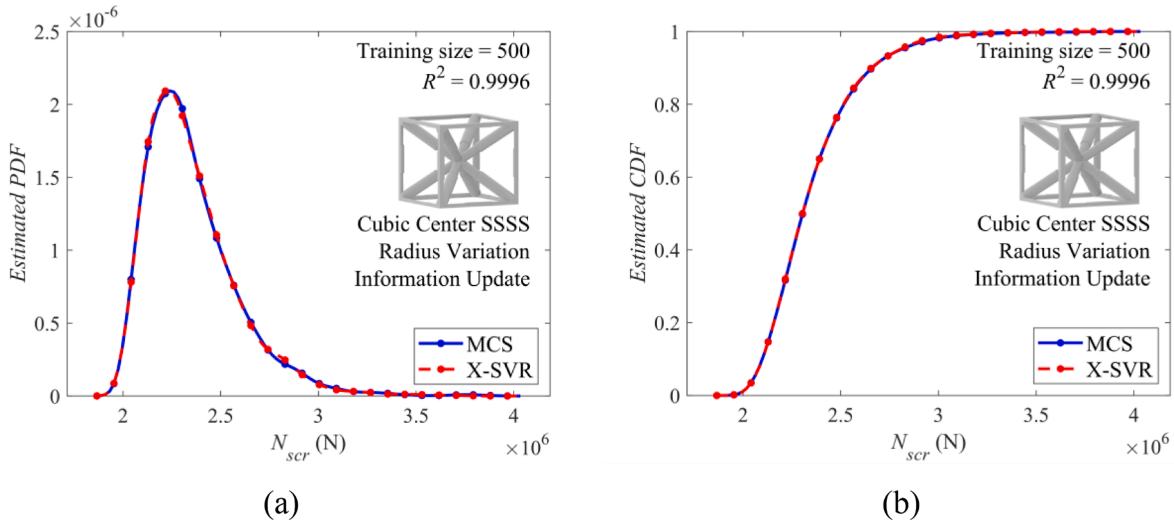

Fig. 11. Estimated statistical results of the cubic center core composite sandwich plate for information update: (a) PDF for radius variation; (b) CDF for radius variation.

Table 11
Estimated probability of N_{scr} for the information update of the simply supported cubic center core composite sandwich plate with radius variation.

Probability	MCS	X-SVR
$P(N_{scr} \leq \mu - 3\sigma)$	0.000000	0.000000
$P(N_{scr} \leq \mu - 2\sigma)$	0.000113	0.000126
$P(N_{scr} \leq \mu - \sigma)$	0.130075	0.131226
$P(N_{scr} \leq \mu)$	0.584582	0.583435
$P(N_{scr} \leq \mu + \sigma)$	0.855965	0.854094
$P(N_{scr} \leq \mu + 2\sigma)$	0.953090	0.951719
$P(N_{scr} \leq \mu + 3\sigma)$	0.986110	0.986805
$P(N_{scr} \leq N_{scr(o)})$	0.955740	0.957352
μ(N)	2351041.68	2349937.53
σ(N)	233244.89	232993.14
σ/μ	0.099209	0.098723

ities, the mean value, and the standard deviation of the static buckling load calculated from X-SVR and MCS in Table 11, the applicability of the proposed analysis framework could be further illustrated, where the random variables can be imported continuously without rebuilding the virtual model. In addition, by observing the results of $N_{scr} \leqslant N_{scr(o)}$, the estimated probability is about 95.5%, which indicates that the static buckling capacity of cubic center composite sandwich plates can be greatly impaired when considering different types of probability distributions together.

5. Conclusion

In this work, a machine learning-aided stochastic analysis framework is proposed for quantifying the effects of AM errors on the static buckling behaviour of composite sandwich plates, including strut node dislocation, radius variation, and waviness. The method of homogenization and the first-order shear deformation theory are combined to create the theoretical basis. Then, a newly developed stochastic analysis framework by adopting extended Support Vector Regression (X-SVR) approach is used for plates with AM errors. To demonstrate the accuracy and efficiency of the proposed framework, the R^2 value, *NRMSE,* and computational time are calculated for the trained models regarding each type of AM error. The statistical information computed from X-SVR and MCS is compared together to further illustrate the applicability of the proposed methodology. Then, the numerical experiments are conducted for the static buckling behaviour of cubic center, octet and vintiles composite plates, which provides new insights into the influence of AM errors on the structural stability and guidance on the structure design and optimization. The conclusions drawn from this work can be summarised herein:

1. The proposed framework through kernelized X-SVR is capable of analysing different types of lattice-core composite sandwich plates and it possesses high robustness for conducting the analysis of static buckling behaviour considering various types of manufacturing imperfections, including strut node dislocation, radius variation, and waviness.
2. The proposed framework greatly increases computational efficiency, and the calculation time can be dramatically reduced without compromising the accuracy of the calculation results.
3. The inherent feature of information update enables the statistical information from different manufacturing sectors to be updated continuously into the analysis framework without rebuilding the trained machine learning model.
4. The influence of AM errors on the static buckling behaviour of composite sandwich plates is more evident than that from boundary condition types.
5. The strut node dislocation possibly increases the overall static buckling capacity for the cubic center core composite sandwich plate, while reducing those from its counterparts made of octet and vintiles cores.

CRediT authorship contribution statement

Weizhe Tian: Conceptualization, Formal analysis, Investigation, Methodology, Software, Validation, Visualization, Writing - original draft, Writing - review & editing. **Qingya Li:** Conceptualization, Methodology, Writing - review & editing. **Qihan Wang:** Conceptualization, Investigation, Methodology, Software, Writing - review & editing. **Da Chen:** Conceptualization, Writing - review & editing. **Wei Gao:** Conceptualization, Funding acquisition, Methodology, Resources, Supervision, Writing - review & editing.

Declaration of Competing Interest

The authors declare that they have no known competing financial interests or personal relationships that could have appeared to influence the work reported in this paper.

Data availability

Data will be made available on request.

Acknowledgements

The work presented in this paper has been supported by Australian Research Council projects IH210100048, IH200100010, DP210101353 and DP240102559.

Appendix A

The admissible functions $X_m(x)$ and $Y_n(y)$ for (SSSS) are expressed as:

$$\begin{aligned} X_m(x) &= \sin(m\alpha x) \\ Y_n(y) &= \sin(n\beta y) \end{aligned} \tag{A1}$$

The admissible functions $X_m(x)$ and $Y_n(y)$ for (CCCC) are expressed as:

$$\begin{aligned} X_m(x) &= \sin(\alpha x)\sin(m\alpha x) \\ Y_n(y) &= \sin(\beta y)\sin(n\beta y) \end{aligned} \tag{A2}$$

Γ_{N11} can be formulated as:

$$\Gamma_{N11} = \int_0^{L_b}\int_0^{L_a}\left\{\left[X_{m,xx}Y_n\right]X_mY_n\right\}dxdy \tag{A3}$$

Appendix B

The coefficient in $\boldsymbol{\Gamma}$ (i.e., Γ_{ij}, for $i, j = 1, 2, 3$) in Eq.(8) can be formulated as:

$$\begin{aligned} \Gamma_{11} &= \int_0^{L_b}\int_0^{L_a}\left\{\left[K_sA_{55}X_{m,xx}Y_n + K_sA_{44}X_mY_{n,yy}\right]X_mY_n\right\}dxdy \\ \Gamma_{12} &= \int_0^{L_b}\int_0^{L_a}\left\{\left[K_sA_{55}X_{m,xx}Y_n\right]X_mY_n\right\}dxdy \\ \Gamma_{13} &= \int_0^{L_b}\int_0^{L_a}\left\{\left[K_sA_{44}X_mY_{n,yy}\right]X_mY_n\right\}dxdy \end{aligned} \tag{B1}$$

$$\begin{aligned} \Gamma_{21} &= \int_0^{L_b}\int_0^{L_a}\left\{\left[-K_sA_{55}X_{m,x}Y_n\right]X_{m,x}Y_n\right\}dxdy \\ \Gamma_{22} &= \int_0^{L_b}\int_0^{L_a}\left\{\begin{bmatrix} \left(B_{11}A_{11}^* + B_{12}A_{12}^* - B_{66}A_{31}^*\right)T_{2,xyy} + \left(B_{11}A_{12}^* + B_{12}A_{22}^*\right)T_{2,xxx} \\ -K_sA_{55}X_{m,x}Y_n + \left(B_{66}A_{32}^* + D_{66}\right)X_{m,x}Y_{n,yy} \\ +\left(B_{11}A_{13}^* + B_{12}A_{23}^* + D_{11}\right)X_{m,xxx}Y_n \end{bmatrix}X_{m,x}Y_n\right\}dxdy \\ \Gamma_{23} &= \int_0^{L_b}\int_0^{L_a}\left\{\begin{bmatrix} \left(B_{11}A_{11}^* + B_{12}A_{12}^* - B_{66}A_{31}^*\right)T_{3,xyy} + \left(B_{11}A_{12}^* + B_{12}A_{22}^*\right)T_{3,xxx} \\ +\left(B_{11}A_{14}^* + B_{12}A_{24}^* + D_{12} + B_{66}A_{32}^* + D_{66}\right)X_{m,x}Y_{n,yy} \end{bmatrix}X_{m,x}Y_n\right\}dxdy \end{aligned} \tag{B2}$$

$$\begin{aligned} \Gamma_{31} &= \int_0^{L_b}\int_0^{L_a}\left\{\left[-K_sA_{44}\Phi_m\Psi_{n,y}\right]X_mY_{n,y}\right\}dxdy \\ \Gamma_{32} &= \int_0^{L_b}\int_0^{L_a}\left\{\begin{bmatrix} \left(B_{12}A_{11}^* + B_{22}A_{12}^*\right)T_{2,yyy} + \left(B_{12}A_{12}^* + B_{22}A_{22}^* - B_{66}A_{31}^*\right)T_{2,xxy} \\ +\left(B_{12}A_{13}^* + B_{22}A_{23}^* + D_{12} + B_{66}A_{32}^* + D_{66}\right)X_{m,xx}Y_{n,y} \end{bmatrix}X_mY_{n,y}\right\}dxdy \\ \Gamma_{33} &= \int_0^{L_b}\int_0^{L_a}\left\{\begin{bmatrix} \left(B_{12}A_{11}^* + B_{22}A_{12}^*\right)T_{3,yyy} + \left(B_{12}A_{12}^* + B_{22}A_{22}^* - B_{66}A_{31}^*\right)T_{3,xxy} \\ -K_sA_{44}X_mY_{n,y} + \left(B_{66}A_{32}^* + D_{66}\right)X_{m,xx}Y_{n,y} \\ +\left(B_{12}A_{14}^* + B_{22}A_{24}^* + D_{22}\right)X_mY_{n,yyy} \end{bmatrix}X_mY_{n,y}\right\}dxdy \end{aligned} \tag{B3}$$

where T_i can be calculated based on the considered boundary conditions [6], $T_{i,x}$ denotes the first derivative of T_i with respect to x, and A_{ij}^* is calculated in the form of:

$$\begin{aligned} &A_{11}^* = \frac{A_{22}}{A_{22}A_{11} - A_{12}^2}, A_{12}^* = -\frac{A_{12}}{A_{22}A_{11} - A_{12}^2}, A_{13}^* = \frac{A_{12}B_{12} - A_{22}B_{11}}{A_{22}A_{11} - A_{12}^2}, \\ &A_{14}^* = \frac{A_{12}B_{22} - A_{22}B_{12}}{A_{22}A_{11} - A_{12}^2}, A_{22}^* = \frac{A_{11}}{A_{22}A_{11} - A_{12}^2}, A_{23}^* = \frac{A_{12}B_{11} - A_{11}B_{12}}{A_{22}A_{11} - A_{12}^2}, \\ &A_{24}^* = \frac{A_{12}B_{12} - A_{11}B_{22}}{A_{22}A_{11} - A_{12}^2}, A_{31}^* = \frac{1}{A_{66}}, A_{32}^* = -\frac{B_{66}}{A_{66}} \end{aligned} \tag{B4}$$

References

[1] Schaedler TA, Carter WB. Architected cellular materials. Annu Rev Mat Res 2016;46:187–210.
[2] Mao A, Zhao N, Liang Y, Bai H. Mechanically efficient cellular materials inspired by cuttlebone. Adv Mater 2021;33(15):2007348.
[3] Hunt CJ, Morabito F, Grace C, Zhao Y, Woods BK. A review of composite lattice structures. Compos Struct 2022;284:115120.
[4] Yang J, Xu R, Hu H, Huang Q, Huang W. Structural-Genome-Driven computing for composite structures. Compos Struct 2019;215:446–53.
[5] Duarte I, Peixinho N, Andrade-Campos A, Valente R. Special issue on cellular materials. Sci Technol Mater 2018;30(1):1–3.
[6] Li Q, Tian W, Wu D, Gao W. Nonlinear dynamic stability analysis of imperfect architected cellular sandwich plate under impact loading. Acta Mech Sin 2023;39(4):722333.
[7] Benedetti M, Du Plessis A, Ritchie RO, Dallago M, Razavi SMJ, Berto F. Architected cellular materials: A review on their mechanical properties towards fatigue-tolerant design and fabrication. Mater Sci Eng R Rep 2021;144:100606.
[8] Prabhu S, Raja VB, Nikhil R. Applications of cellular materials–an overview. Appl Mech Mater 2015;766:511–7.
[9] Li P, Yang F, Bian Y, Zhang S, Wang L. Designable mechanical properties of modified body-centered cubic lattice materials. Compos Struct 2023;317:117060.
[10] Czerwinski F. Current trends in automotive lightweighting strategies and materials. Materials 2021;14(21):6631.
[11] Chuang WANG, Jihong ZHU, Manqiao WU, Jie HOU, Han ZHOU, Lu MENG, et al. Multi-scale design and optimization for solid-lattice hybrid structures and their application to aerospace vehicle components. Chin J Aeronaut 2021;34(5):386–98.
[12] Gorguluarslan RM, Choi SK, Saldana CJ. Uncertainty quantification and validation of 3D lattice scaffolds for computer-aided biomedical applications. J Mech Behav Biomed Mater 2017;71:428–40.
[13] Chica L, Alzate A. Cellular concrete review: New trends for application in construction. Constr Build Mater 2019;200:637–47.
[14] Leary M, Merli L, Torti F, Mazur M, Brandt M. Optimal topology for additive manufacture: A method for enabling additive manufacture of support-free optimal structures. Mater Des 2014;63:678–90.
[15] Gardan J. Additive manufacturing technologies: state of the art and trends. Int J Prod Res 2016;54(10):3118–32.
[16] Tao, W., & Leu, M. C. (2016, August). Design of lattice structure for additive manufacturing. In *2016 International Symposium on Flexible Automation (ISFA)* (pp. 325-332). IEEE.
[17] Uribe-Lam E, Treviño-Quintanilla CD, Cuan-Urquizo E, Olvera-Silva O. Use of additive manufacturing for the fabrication of cellular and lattice materials: a review. Mater Manuf Process 2021;36(3):257–80.
[18] Guo N, Leu MC. Additive manufacturing: technology, applications and research needs. Front Mech Eng 2013;8:215–43.
[19] Leary M, Mazur M, Elambasseril J, McMillan M, Chirent T, Sun Y, et al. Selective laser melting (SLM) of AlSi12Mg lattice structures. Mater Des 2016;98:344–57.
[20] Novak N, Vesenjak M, Krstulović-Opara L, Ren Z. Mechanical characterisation of auxetic cellular structures built from inverted tetrapods. Compos Struct 2018;196:96–107.
[21] Lozanovski B, Leary M, Tran P, Shidid D, Qian M, Choong P, et al. Computational modelling of strut defects in SLM manufactured lattice structures. Mater Des 2019;171:107671.
[22] Bikas H, Stavropoulos P, Chryssolouris G. Additive manufacturing methods and modelling approaches: a critical review. Int J Adv Manuf Technol 2016;83:389–405.
[23] Maconachie T, Leary M, Lozanovski B, Zhang X, Qian M, Faruque O, et al. SLM lattice structures: Properties, performance, applications and challenges. Mater Des 2019;183:108137.
[24] Song J, Gao L, Cao K, Zhang H, Xu S, Jiang C, et al. Metal-coated hybrid meso-lattice composites and their mechanical characterizations. Compos Struct 2018;203:750–63.
[25] Yuan L, Ding S, Wen C. Additive manufacturing technology for porous metal implant applications and triple minimal surface structures: A review. Bioact Mater 2019;4:56–70.
[26] Gardner, L. (2023, January). Metal additive manufacturing in structural engineering–review, advances, opportunities and outlook. In *Structures* (Vol. 47, pp. 2178-2193). Elsevier.
[27] Bici M, Brischetto S, Campana F, Ferro CG, Seclì C, Varetti S, et al. Development of a multifunctional panel for aerospace use through SLM additive manufacturing. Procedia Cirp 2018;67:215–20.
[28] Frazier WE. Metal additive manufacturing: a review. J Mater Eng Perform 2014;23:1917–28.
[29] Dallago M, Winiarski B, Zanini F, Carmignato S, Benedetti M. On the effect of geometrical imperfections and defects on the fatigue strength of cellular lattice structures additively manufactured via Selective Laser Melting. Int J Fatigue 2019;124:348–60.
[30] Liu L, Kamm P, García-Moreno F, Banhart J, Pasini D. Elastic and failure response of imperfect three-dimensional metallic lattices: the role of geometric defects induced by Selective Laser Melting. J Mech Phys Solids 2017;107:160–84.
[31] Lei H, Li C, Meng J, Zhou H, Liu Y, Zhang X, et al. Evaluation of compressive properties of SLM-fabricated multi-layer lattice structures by experimental test and μ-CT-based finite element analysis. Mater Des 2019;169:107685.
[32] Cao X, Jiang Y, Zhao T, Wang P, Wang Y, Chen Z, et al. Compression experiment and numerical evaluation on mechanical responses of the lattice structures with stochastic geometric defects originated from additive-manufacturing. Compos B Eng 2020;194:108030.
[33] Yang Y, Hui Y, Li P, Yang J, Huang Q, Giunta G, et al. Global/local buckling analysis of thin-walled I-section beams via hierarchical one-dimensional finite elements. Eng Struct 2023;280:115705.
[34] Dong G, Tang Y, Zhao YF. A 149-line homogenization code for three-dimensional cellular materials written in matlab. J Eng Mater Technol 2019;141(1).
[35] Hassani B, Hinton E. A review of homogenization and topology optimization I—homogenization theory for media with periodic structure. Comput Struct 1998;69(6):707–17.
[36] Qolipour AM, Eipakchi H, Nasrekani FM. Asymmetric/Axisymmetric buckling of circular/annular plates under radial load using first-order shear deformation theory. Thin-Walled Struct 2023;182:110244.
[37] Wang Q, Li Q, Wu D, Yu Y, Tin-Loi F, Ma J, et al. Machine learning aided static structural reliability analysis for functionally graded frame structures. App Math Model 2020;78:792–815.
[38] Wang Q, Wu D, Tin-Loi F, Gao W. Machine learning aided stochastic structural free vibration analysis for functionally graded bar-type structures. Thin-Walled Struct 2019;144:106315.
[39] Wang Q, Wu D, Li G, Gao W. A virtual model architecture for engineering structures with Twin Extended Support Vector Regression (TX-SVR) method. Comput Methods Appl Mech Eng 2021;386:114121.
[40] Wang Q, Feng Y, Wu D, Li G, Liu Z, Gao W. Polymorphic uncertainty quantification for engineering structures via a hyperplane modelling technique. Comput Methods Appl Mech Eng 2022;398:115250.
[41] Wang L, Zhu J, Zou H. The doubly regularized support vector machine. Stat Sin 2006:589–615.
[42] Scholkopf B, Mika S, Burges CJ, Knirsch P, Muller KR, Ratsch G, et al. Input space versus feature space in kernel-based methods. IEEE Trans Neural Netw 1999;10(5):1000–17.